Meteorology and Atmospheric Physics (2021) 133:857–878
https://doi.org/10.1007/s00703-021-00780-7

ORIGINAL PAPER

Evaluation of 3D structural changes in general atmospheric and monsoon circulations during Kedarnath disaster (India), 16–17 June 2013

Ranade Ashwini[1] · **Singh Nityanand**[2,3]

Received: 28 April 2020 / Accepted: 24 January 2021 / Published online: 25 February 2021

Abstract

Intense rains on 16–17 June 2013 over Mandakini River catchment caused Kedarnath disaster in Uttarakhand State (India). Normal and departure-from-normal 3D global atmospheric thermal structure and general and monsoon circulations during the event have been compared using equatorially/globally- conditioned surface and upper air parameters (1000–100 hPa) (period: 1979–2013). Briefly, normal monsoon structure is: *1000–850 hPa layer*- cross-equatorial flows over Indian Ocean and Eurasian westerlies confluence over Indian domain, the two flows further confluence downstream with Pacific easterlies and then the accumulated airmasses blow northeastward; *700–500 hPa layer*- Eurasian westerlies after sweeping entire Indian subcontinent make exit northeastward; and *400–100 hPa layer*- upper tropospheric anticyclone well-developed over subtropical Asia and outflows are spread all around. On 16–17 June 2013, two upper tropospheric anticyclonic cells occurred, one over Tibet-China and another Mediterranean-Middle East. Troposphere (1000–250 hPa) was significantly warmer-and-thicker over Tibet-China followed by Mediterranean-Middle East while cooler-and-thinner over central Asia-India sector. Departures in downward slopes of tropospheric temperature and thickness from Tibet-China outward were significantly steeper. A huge trough evolved over Indo-Pacific region from an interaction between Eurasian westerlies and Indo-Pacific easterlies, and outflows from the trough made forced exit through western Himalaya which modulated north mid-high latitudes westerlies into a single wave structure. Combined five factors produced disastrous rains over Kedarnath: cool-low and warm-low regime contrast; squeezing of deep warm-moist flows; orographic lifting; and pumping and suction effects. Forced warm-moist outflows from Indo-Pacific region caused warmer-thicker troposphere over eastern Russia-North America. Lesser outflows from Tibet-China anticyclone were directed southward, consequently troposphere was cooler-thinner over southern mid-high latitudes.

Abbreviations

AIP	Asia-Indo-Pacific
CA-IND	Central Asia – India
CH	Cool-high
CL	Cool-low
EC-mslp	Equatorially Conditioned mean sea level pressure
EC-PW	Equatorially Conditioned Precipitable Water
EC-T_{level}	Equatorially Conditioned Temperature at particular level
EC-T_{TROP}	Equatorially Conditioned Tropospheric temperature
EC-Z_{level}	Equatorially Conditioned geopotential height at particular level
EC-Z_{TROP}	Equatorially Conditioned Tropospheric Thickness
EMV	Equatorial Mean Value
EREs	Extreme Rain Events
GC-W	Globally Conditioned Wind Speed
GMV	Global Mean Value
GWRs	Global Weather Regimes
LOSSI	Location, orientation, shape, size and intensity

Responsible Editor: Silvia Trini Castelli.

✉ Ranade Ashwini
ranadeashwini@gmail.com

Singh Nityanand
singhnityanand@gmail.com

[1] Surface Water Hydrology Division, National Institute of Hydrology, Roorkee, Uttarakhand 247667, India

[2] Indian Institute of Tropical Meteorology, Dr. Homi Bhabha Road, Pashan, Pune, Maharashtra 411008, India

[3] 9, Pashan Villa, Pashan, Pune, Maharashtra 411021, India

MME	Mediterranean – Middle East
NH	Northern Hemisphere
NPL	North Polar
NSBT	North Subtropic
SH	Southern Hemisphere
SPL	South Polar
SSBT	South Subtropic
TBT-CHN	Tibet-China
WL	Warm-low
WH	Warm-high

1 Introduction

Kedarnath town (30° 44′ N, 79° 04′ E; 3553 m a.s.l.) in Indian state of Uttarakhand (area: 53,566 km^2) is situated on the bank of the Mandakini River in the backdrop of Kumaun Himalaya physiographic division (NATMO 1986). The town is famous for a holy Kedarnath shrine and visited by large number of devotees (sometimes exceed 100,000 per day) during May–October. The Saraswati River joins the Mandakini River in upstream. During 15–18 June 2013, a steep mountainous catchment of the Mandakini River (area: ~ 67 km^2; altitudinal variation 2740–6940 m) received continuous rains, very heavy rains occurred on 16–17 June 2013 (Dobhal et al. 2013). Meteorological observatory of the Wadia Institute of Himalayan Geology (WIHG), India, about 2 km in upstream of the Kedarnath town, reported 325 mm of rainfall between 15 June (5:00 pm, IST) and 16 June 2013 (5:00 pm, IST) (Dobhal et al. 2013). Ray et al. (2016) provided distribution of number of rain reporting raingauges and rainfall amount across the Uttarakhand state on each day of 16–18 June 2013 (16 June: 16 raingauges, 70–220 mm;17 June: 24 raingauges, 80–370 mm; and 18 June: 16 raingauges, 70–280 mm). Due to sparse raingauge network and limited radar coverage, satellite imageries and satellite-derived precipitation estimates have also been used to understand the fury of the heavy rainfalls (Parida et al. 2017; Mishra and Srinivasan 2013). Vellore et al. (2019) documented 24-h (ending 0300 UTC 17 June 2013) total rainfall of 38 raingauges across Uttarakhand region which showed variation in the range 43 mm (Ramnagar, elevation 1700 m) to 410 mm (Purola, elevation 1503 m). Positive correlation between elevation and rainfall amount was not seen during the event. Figure 1 shows daily rainfall distribution across extreme northern India from 15 June through 18 June 2013. The figure is prepared using 0.5°-gridded daily rainfall from the dataset developed and updated by the India Meteorological Department, details are given in Rajeevan and Bhate (2008). Heavy to very heavy rainfall occurred on 16–17 June 2013 in and around Kedarnath town, the core of highest rainfall was located in west and north directions of the town. Broad spatial features of the daily rainfall from 15 June through 18 June 2013 were: overall increase in rainfall amount and spatial extent up to 17 June, and decrease thereafter while shifting eastward. Kedarnath and the catchment area in its upstream received 40–130 mm of rainfall on 16–17 June 2013. Considerable rains also occurred over Himachal Pradesh, Haryana, Delhi and Utter Pradesh, western Nepal as well as parts of Tibet (Dubey et al. 2013; Vellore et al. 2019). Besides flooding, heavy rains caused river channel shift and bank erosion, landslides and accumulation of debris in the river channels which further aggravated the situation, resulting in immeasurable losses to life and property, and damages to human and natural ecosystems (Mishra and Srinivasan 2013; Martha et al. 2015). Kedarnath town suffered maximum causalities, damages and losses, hence, referred to as Kedarnath disaster (Dobhal et al. 2013). An elaborate description of losses and destructions during the event due to natural and anthropogenic factors is given in Dubey et al. (2013) and Sati (2013). It was considered among the worst natural disaster in recent decades in the country.

Researchers have suggested occurrence of several synoptic scale, mesoscale and microscale weather systems/fields/processes embedded in unusually large and intense monsoon trough as causal factors for unprecedented rainfall over Kedarnath area (Srinivasan 2013; Dube et al. 2014; Kotal et al. 2014; Joseph et al. 2015; Vellore et al. 2016; Houze et al. 2017; Priya et al. 2017). Several investigators emphasized the considerable role of moisture advection from Arabian Sea and Bay of Bengal into monsoon system and orographic lifting of moist airflows along a steep slope of the western Himalaya (Dube et al. 2014; Kotal et al. 2014; Singh et al. 2014; Joseph et al. 2015; Vellore et al. 2016; Ranalkar et al. 2016; Houze et al. 2017; Krishnamurti et al. 2017). While others felt/conjectured critical role of processes like quasi-stationary regeneration of mesoscale convective systems along the zone of convergence (Kotal et al. 2014), stronger than normal vertical easterly wind shear during early-June (Singh et al. 2014), anomalously warmer highlands (~ 2 standard deviations), record-low Eurasian snow cover (NOAA 2013) and colder upper troposphere over the Arctic region (Joseph et al. 2015), intense winds from Arabian Sea (Priya et al. 2017), eddy shedding of Tibetan anticyclone (Vellore et al. 2016), buildup of potential buoyancy and strong vertical acceleration (Krishnamurti et al. 2017), and supply of vorticity sources to monsoon environment by slow-moving deep westerly trough which supported persistent extratropical-monsoon interactions and rainfall over Uttarakhand region (Vellore et al. 2019). Numerical modelling studies have attempted to simulate as well as predict the Kedarnath event, and reported satisfactory results (Dube et al. 2014; Joseph et al. 2015; Shekhar et al. 2015; Cho et al. 2015; Chevuturi and Dimari 2016 and others).

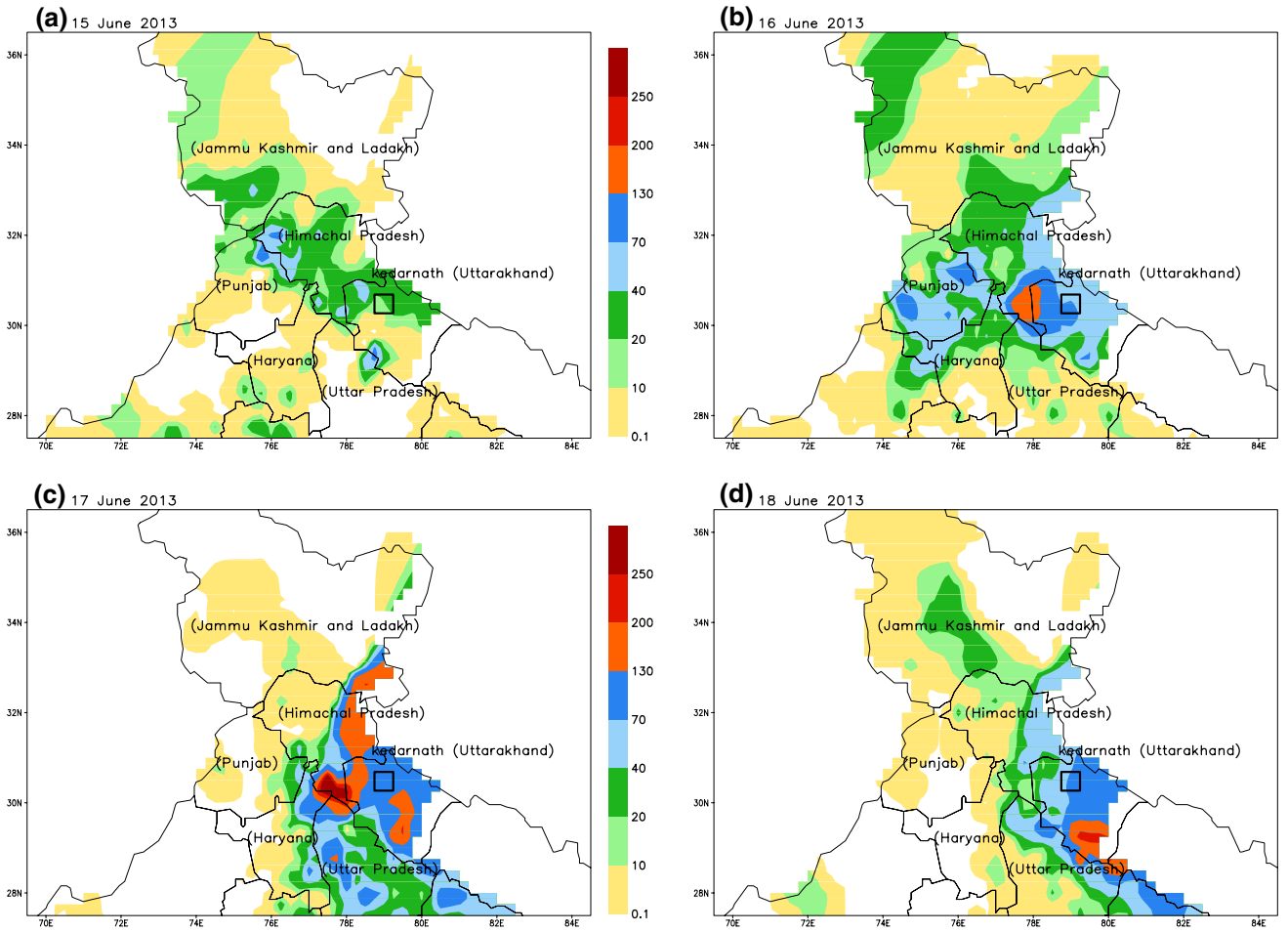

Fig. 1 Daily rainfall distribution across part of northern India during 15–18 June 2013 (India Meteorological Department; details in Rajeevan and Bhate 2008)

Besides these, number of studies were undertaken keeping in view report of the International Disaster Database (http://www.emdat.be) which suggested a substantial increase in the extreme rain events (EREs) over western Himalayas in recent 30–40 years. Notable EREs studies of the Himalayan region are: 27–30 July 2010 over Pakistan (Hong et al. 2011; Houze et al. 2011; Lau and Kim 2012; Webster et al. 2011), 4–6 Aug 2010 over Leh (Ladakh, India) and surrounding region of Ladakh (Ashrit 2010; Rasmussen and Houze 2012; Thayyen et al. 2013; Kumar et al. 2014), 19 July 2007 over central Nepal (Bohlinger et al. 2019), 3 August 2012 over Uttarkashi (Chaudhari et al. 2015) and 13–14 September 2012 over Rudraprayag (Chevuturi et al. 2015). Furthermore, Vellore et al. (2016) analyzed synoptic features of 34 EREs over western Himalaya since 1979, Rasmussen et al. (2015) described large-scale and mesoscale characteristics of different storms during 2010–2012, and Bohlinger et al. (2017) analyzed composite of the events over Nepal during 1979–2010. Therefore, multiple visualizable factors operated in unison to produce extreme weather/rain events across subtropical Asia in general and during Kedarnath disaster in particular. Notable features of the monsoon circulation from aforementioned studies can be broadly grouped into three categories: (1) evolution of large and intense monsoon trough from interactions between unusually deep westerly trough and cross-equatorial Indian Ocean southwesterlies as well as Pacific easterlies; (2) excessive moisture advection into monsoon regime from Arabian Sea and Bay of Bengal; and (3) evolution of numerous synoptic scales, mesoscale and microscale weather systems/fields/processes embedded in anomalous monsoon trough. An attempt has been made to demonstrate the following.

- There was a short period change in general and monsoon circulations caused by anomalous change in the global atmospheric temperature structure;
- There was unprecedented interaction between deep westerly trough and lower tropospheric monsoon circulation resulting in evolution of unusually intense and large mon-

soon trough, extending from Philippine through Indus basin; and
- Synoptic scale, mesoscale and microscale weather systems/fields/processes embedded in the monsoon trough, as well as those, occurred outside monsoon regime were interconnected.

Earlier, the authors (Ranade and Singh 2019) have analyzed series of customized global charts of selected atmospheric parameters to understand time-evolution of 3D structural changes in general and monsoon circulations that caused heaviest monsoon rains over India during 23–28 July 2005, and Mumbai disaster on 26–27 July 2005. The approach has been adopted to evaluate changes in global atmospheric temperature and general and monsoon circulations as well as to understand underlying mechanism that produced very heavy rains on 16–17 June 2013 over Kedarnath area. Brief description of different types of conditioning to prepare customized global charts has been given in Sect. 3. Life-cycle of the of the monsoon circulation has been briefly described in Sect. 4. Normal structure of global atmospheric thermal condition and general as well as monsoon circulations on 16–17 June has been described in Sect. 5, and actual on 16–17 June 2013 in Sect. 6. An elaboration of the underlying mechanism of the great disaster has been provided in Sect. 7, and a summary and concluding remark thereafter in Sect. 8.

2 Data used

For the period 1979–2013, six-hourly, 2.5°-gridded global data of pressure (mslp), precipitable water (PW), and temperature (T), geopotential height (Z) and wind (u and v) at 12 selected levels (1000–100 hPa) for the period 1979–2013 have been downloaded from website of the 'The National Centers for Environmental Prediction (NCEP)' Climate Forecast System Reanalysis (CFSR and CFSv2) (Saha et al. 2010, 2014). From arithmetic mean of the 6-hourly values, the daily dataset has been prepared. Half-degree gridded daily rainfall (1979–2013) used in the study has been obtained from the India Meteorological Department (Rajeevan and Bhate 2008).

3 Conditioning, classification and criteria

3.1 Three types of conditioning of the atmospheric parameters used

To understand global atmospheric thermal and circulation changes following north–south seasonal oscillation of the sun, global charts of three types of conditioned atmospheric parameters have been prepared, equatorial, global and self.

3.1.1 Equatorially-conditioned (EC) charts

Zonal mean bounded by the parallels 2.5 °S–2.5 °N, referred to as equatorial mean value (or EMV, Table 1), is subtracted from individual grid-cell across the globe, and isolines are drawn. The equator is characterized by least seasonal and a

Table 1 16–17 June mean and SD of the equatorial mean value (EMV, zonal mean of 2.5°S–2.5°N) of levelwise (1000–100 hPa) temperature and geopotential height, and global mean value (GMV) of wind speed

Level (hPa)	Temperature (°C)		Height/thickness (m)		Wind speed (m/s)	
	Mean EMV	S.D	Mean EMV	S.D	Mean GMV	S.D
1000	26.1	0.3	97.6	6.3	5.3	0.2
925	21.2	0.3	779.1	6.1	6.5	0.2
850	17.1	0.3	1507.4	6.1	6.8	0.3
700	8.8	0.4	3139.9	6.5	7.8	0.3
600	2.7	0.5	4403.1	7.2	8.7	0.3
500	−5.0	0.4	5857.2	8.4	9.4	0.3
400	−15.8	0.5	7575.9	10.7	11.0	0.4
300	−31.6	0.6	9677.3	15.3	13.9	0.4
250	−41.8	0.6	10,939.2	18.4	15.6	0.4
200	−53.8	0.6	12,411.0	22.3	16.2	0.5
150	−67.4	0.6	14,198.7	26.6	15.0	0.6
100	−78.5	0.9	16,561.3	26.8	9.8	0.7
T_{TROP}	−2.0	0.4	10,841.6	18.9	9.4	0.2

The parameters for the troposphere are given in the last row. Data used: 1979–2013

minimum diurnal variation, hence the EMV is natural and a robust reference. The EC charts are useful of the parameters which display general increasing/decreasing pattern from the equator to the polar regions such as T, Z, PW etc.

3.1.2 Globally-conditioned (GC) charts

Global mean value (GMV, Table 1) is subtracted from individual grid-cell to prepare GC charts of the parameters which show two or more zonal belts of high/low values over the globe, such as pressure (three low pressure and four high pressure belts), wind speed (subtropical and subpolar belts of strong winds) etc. However, comparison of normal daily EC-mslp and GC-mslp charts for the full year did not suggest considerable difference. Furthermore, the EC-mslp is directly useful alongwith EC-T, EC-Z and EC-PW charts to understand spreading and intensification of equatorial atmospheric condition and vertical circulation structure as well as evolution of the monsoon circulation. Hence, the EC-mslp is adopted for detailed analyses.

The standard deviation of the EMV/GMV of T_{level}, Z_{level}, W_{level}, T_{TROP}, Z_{TROP} and W_{TROP} is very small (Table 1) and can be ignored. Mean and standard deviation of the EMV of mslp is 1011.2 mb and 0.7 mb, and that of PW 43.9 mm and 2.0 mm.

3.1.3 Self-conditioned (SC) charts

The respective grid-cell annual mean is subtracted from the grid-cell daily value to prepare SC charts, which are useful to know the status of spreading of warming from equator toward polar region over summer hemisphere and cooling from polar region toward equator over winter hemisphere. During late-May through late-September, warmer-and-thicker troposphere (1000–250 hPa) (SC-T_{TROP} and SC-Z_{TROP} positive) occurs over the northern hemisphere (NH) and cooler-and-thinner (SC-T_{TROP} and SC-Z_{TROP} negative) over the southern Hemisphere (SH).

3.2 Global weather regimes (GWRs)

Parallel comparison of level-wise daily EC-T_{level} and EC-Z_{level} charts suggests that EC-Z_{level} could be positive as well as negative for corresponding EC-T_{level} both positive or negative. Therefore, considering each of EC-T_{level} and EC-Z_{level} in two attributes (positive/negative or + ve/–ve) four types of weather regimes are identified across the globe as: warm-low (WL; EC-T_{level} + ve and EC-Z_{level} –ve), warm-high (WH; both EC-T_{level} and EC-Z_{level} + ve), cool-low (CL; both EC-T_{level} and EC-Z_{level} –ve) and cool-high (CH; EC-T_{level} –ve and EC-Z_{level} + ve) (Ranade and Singh 2019). Collectively they are referred to as global weather regimes (GWRs). Characteristics of upper and lower levels large-scale features of circulations in each of the four regimes are documented in Ranade and Singh (2019). Levelwise display of the GWRs, streamlines and GC-W_{level} for full depth of the atmosphere (1000–100 hPa) provide adequate visually interpretable charts to get insight into 3D structure of the monsoon circulation embedded in the general atmospheric circulation.

3.3 Area under Indian monsoon condition

The monsoon is a rain-producing weather system, two additional parameters pressure and PW are considered to refine the warm-low regime to demarcate the area under Indian monsoon condition (AUIMC) conducive for the occurrence of frequent large-scale rain-spells. Therefore, the final criterion for demarcation of the AUIMC is as: EC-$T_{1000–700}$ and EC-PW + ve, and EC-Z_{600} and EC-mslp –ve. Important to note that Eurasian westerlies (portion of north mid-latitude westerlies blowing over Eurasia) enter into Indian domain (Arabian Sea–India–Bay of Bengal) after breaking off the subtropical high-pressure belt over the Middle East – extreme northern India (EC-Z_{level} negative of the lower tropospheric levels), either due to warming or cooling of the lower tropospheric levels. Over the region, lowering of the height of lower-lower levels (1000–700 hPa) due to warming (EC-T_{level} + ve) and that of lower–upper levels (600–500 hPa) due to cooling is frequently observed. Furthermore, the height of the 500 hPa in not clearly lower than the equator except when the monsoon is intense. Keeping in view these situations, the conditions EC-$T_{1000–700}$ positive and EC-Z_{600} negative are considered in the criteria.

3.4 Troposphere and upper levels

The levelwise normal daily EC-T_{level} charts show, polar regions cooler than the equator up to 250 hPa throughout the year. The layer 1000–250 hPa is, therefore, considered as troposphere, and three levels above 250 hPa (200, 150 and 100 hPa) as upper levels which are warmer over polar regions during respective summer. Tropospheric temperature and thickness are examined to understand global-scale departure/change in the atmospheric thermal condition. Temperature and height of the upper levels are analyzed separately.

4 Life cycle of the monsoon circulation

Monsoon is a massive thermally direct tropical circulation system which produces summer seasonal rainfall across Asia-Indo-Pacific region (AIP: Eq. – 50 °N; 50°–150°E). During boreal summer (austral winter), there is massive reorganization of the components of the general atmospheric circulation (different climatic zones and ‘centers of

action') characterized by changes in their location, orientation, shape, size and intensity (LOSSI). We understand that the monsoon evolves in association with spreading and intensification of equatorial atmospheric thermal condition (warmest-thickest troposphere and lowest pressure), vertical circulation structure (lower tropospheric confluence/convergence and upper tropospheric difluence/divergence) and highest precipitable water (Ranade and Singh 2019). Heating, upward motion, increased lapse-rate, inflows in lower troposphere and outflows from upper troposphere, and cyclonic/anticyclonic curvature/circulation as well as embedded multiscale weather systems increase over northern tropic-subtropic, and decrease over southern tropic-subtropic while cooling, downward motion, horizontal temperature gradient, inflow in upper troposphere and return flows in lower troposphere, waves, fronts, and forced cyclonic/anticyclonic curvature and convergence/divergence related dynamism decrease over northern mid-high latitudes and increase over southern mid-high latitudes. Starting from late-March, the changes attain peak and plateauing condition during late-July-and-early-August. Two important seasonal changes that are directly associated with the evolution of the monsoon are: (1) northward shift of north subtropical ridge from ~ 20 °N over Africa–Arabian Sea–India–North Pacific sector to ~ 35 °N and its division into two intense anticyclonic circulations—North Pacific high and Mediterranean—western Middle East high; and occurrence of a huge low-pressure field (lower than the EMV) extending across equator – AIP – Asian landmass – north polar. The core of the monsoon circulation is located over subtropical Asia (Tibet-Himalaya-Middle East sector) with warmest-thickest troposphere, lowest pressure and biggest zonally-oriented upper tropospheric anticyclonic circulation. Evolution of south Asian phase or Indian monsoon starts around end-May when depth of lower level convergence extends above 850 hPa. To get a mental picture of the Indian monsoon circulation at its peak (end-July), a three layer description of the wind field is given below.

1000–850 hPa: Cross-equatorial flows over Indian Ocean after sweeping Indian domain, part converge over Indo-Gangetic Plains and the remaining confluence with Pacific easterlies over Indochina – South China Sea, and the combined wind blow towards northeast over eastern Asia – Pacific sector which eventually collapse into Aleutian low.

700–500 hPa A part of Eurasian westerlies (a portion of north mid-high latitudes westerlies over Eurasia) divert through the Middle East into Indian domain, and evolve into a huge whirlpool type cyclonic circulation (monsoon trough/convergence zone) after interacting with cross-equatorial Indian Ocean westerlies and Pacific easterlies (combined wind system of straight-flowing North Pacific easterlies and South Pacific easterlies crossing the equator).

400–100 hPa Air converging into monsoon trough and other places around Tibetan plateau rise and accumulate in upper levels over subtropical Asia, spread out across the globe via anticyclonic circulation, subside over subtropical and polar highs and returnflows from lower-layers of the highs eventually converge into monsoon regime completing the cycle.

Three large-scale winds converge over India-Indo-Pacific region: Pacific easterlies (combination of straight-flowing North Pacific easterlies and cross-equatorial South Pacific easterlies; referred to as monsoon easterlies), cross-equatorial Indian Ocean south-westerlies and Eurasian westerlies. The two Pacific easterlies provide moisture to the monsoon system and the westerlies add strength to the monsoon circulation by increasing vertical depth of lower tropospheric cyclonic circulation and convergences (500 hPa and above). This warm-moist wind over Indian domain will be referred to as Indian monsoon wind, and that of entire India-Indo-Pacific region as monsoon regime. An observer experiences different direction of the Indian monsoon wind at different locations within Indian domain due to the circular nature of the lower level winds. Part of the lower tropospheric monsoon circulation converge over Indian domain; part converge over Tibetan plateau and remaining exit towards eastern Asia – Pacific region. Vertical structure of the monsoon circulation consists of two main components: (1) warm-low, moist lower tropospheric convergence covering whole of the AIP; and (2) warm-high upper tropospheric divergence covering whole of subtropical Asia. In lower troposphere, the monsoon trough extending across Bay of Bengal -Indo-Gangetic plains -Indus basin (north of 15 °N) is most important internal organ of the monsoon system. It is a secondary disturbance and during intense monsoon activities smaller perturbances (cyclonic circulation, eddies, vortices etc.) are embedded in the convergence zone which plays crucial role in rainfall production and its space–time distribution. Two important factors that control LOSSI of the monsoon system in general and that of the monsoon trough in particular are: (1) tropospheric temperature and thickness fields over the NH, the SH and the subtropical (particularly Tibetan) Asia, and tropospheric temperature/thickness downward slope from the subtropical Asia outwards; and (2) associated changes in 3D structure of the general and monsoon circulations. The retreat starts around mid-August with southeastward migration of the warmest-thickest troposphere, and the process finishes by end-November.

5 Normal global atmospheric temperature and general and monsoon circulation structures on 16–17th June

5.1 Temperature, height/thickness, pressure and precipitable water

5.1.1 T_{TROP}/Z_{TROP}

A brief outline of global tropospheric temperature/thickness is in order: the EC-T_{TROP}/EC-Z_{TROP} of the NH is − 4.4 °C/− 228.3 m, the SH − 11.6 °C/− 513.2 m, the NPL − 18.1 °C/− 778.3 m and the SPL − 37.1 °C/− 1501.3 m (Fig. 2, Table 2). The north–south temperature/thickness contrast, therefore, is 7.2°/264.9 m. Keeping in view, two anomalously warm cores separated by an anomalously cool core in departure-from-normal tropospheric temperature field during 16–17 June 2013 (Fig. 7), the subtropical Afroeurasia has been divided into three sectors for the present study: Tibet–China (TBT-CHN), Central Asia-India (CA-IND) and Mediterranean – Middle East (MME). Normal 16–17 June EC-T_{TROP} of the TBT-CHN is + 0.4 °C, the CA-IND + 2.1 °C and the MME − 0.9 °C (Table 2).

5.1.2 Upper levels T and Z

At 200 hPa, mild warmer condition (EC-T_{200} positive) occurs over Indo-Pacific, and intense warmer over north mid-high latitudes (north polar > + 12 °C) (Fig. 3). Remaining entire globe experiences cooler condition. Compared to the 200 hPa level, at 150 hPa much larger area experiences warmer condition over northern high latitudes (north polar > + 24 °C). South subtropic is second largest warmer area with multiple cores (> + 12°) across. While cooler condition occurs across the tropics in three isolated pockets and continuous across entire south mid-high latitudes. At 100 hPa, intense warmer condition occurs over major parts of the globe (core > + 36 °C over north polar followed by > + 24 °C over south subtropic) while tropical Indo-Pacific Ocean and south polar experience cooler condition. Global distribution of the upper levels EC-Z display simple pattern with the highest value over subtropical Asia and monotonically decreasing towards the poles. At 200 hPa, core (> + 100 m) is located over central India-Bangladesh, decreases to less than − 800 m (< − 1800 m) over NPL (SPL); at 150 hPa, core (> + 150 m) over southern India-Indochina, decreases to less than − 800 m (< − 1800 m) over NPL (SPL); and at 100 hPa, core (> + 150 m) over Pakistan-India-Tibet, decreases to less than − 200 m (< − 1800 m) over NPL (SPL) (Fig. 3).

Table 2 Normal tropospheric temperature T_{TROP} (EC-T_{TROP}) and thickness Z_{TROP} (EC-Z_{TROP}) and mslp (EC-mslp) during 16–17 June over indicated geographical units, and departure-from-normal (DFN) during 16–17 June 2013

Geographical units	Tropospheric temperature T_{TROP} (°C)		Tropospheric thickness Z_{TROP} (m)		MSLP (mb)	
	Normal (EC-T_{TROP})	DFN	Normal (EC-Z_{TROP})	DFN	Normal (EC-MSLP)	DFN
GLB (globe)	− 10.0 (− 8.0)	+ 0.3	10,497.7 (− 370.7)	+ 13.5	1011.3 (+ 0.1)	0.0
NH (north hemisphere.)	− 6.4 (− 4.4)	+ 0.6	10,640.1(− 228.3)	+ 26.8	1012.1 (+ 0.9)	− 0.7
SH (south hemisphere)	− 13.7 (− 11.6)	− 0.1	10,355.2 (− 513.2)	+ 0.3	1010.5 (− 0.6)	+ 0.7
NPL (north polar) (70°–90°N)	− 20.2 (− 18.1)	0.0	10,090.1 (− 778.3)	− 1.7	1012.2 (+ 1.0)	− 3.9
NMLat (north mid-latitudes) (45°–70°N)	− 13.9 (− 11.8)	+ 0.6	10,328.3 (− 540.1)	+ 21.9	1011.6 (+ 0.5)	+ 0.8
NSBT (north subtropic) (25°–45°N)	− 4.7 (− 2.7)	+ 0.8[5]	10,696.5(− 171.9)	+ 38.4	1014.2 (+ 3.0)	− 0.8
NTP (north tropic) (2.5°–25°N)	− 1.5 (+ 0.6)	+ 0.5	10,853.4 (− 15.0)	+ 24.5	1010.9 (− 0.3)	− 1.0
EQU (equator; 2.5°S–2.5°N)	− 2.0	+ 0.8[5]	10,868.4	+ 9.4[5]	1011.2	− 1.3
STP (south tropic) (2.5°–25°S)	− 3.6 (− 1.6)	+ 0.5	10,775.6 (− 92.8)	+ 27.5	1014.5 (+ 3.7)	− 1.6[5]
SSBT (south subtropic) (25°-45°S)	− 13.9 (− 11.8)	+ 0.1	10,335.1 (− 533.3)	+ 8.9	1017.0 (+ 5.8)	+ 0.5
SMLat (south mid-latitudes) (45°–70°S)	− 25.5 (− 23.4)	− 1.0[5]	9860.1 (− 1008.3)	− 41.4[5]	996.2 (− 15.0)	+ 2.9
SPL (south polar) (70°–90°S)	− 39.1 (− 37.1)	− 1.6	9367.1 (− 1501.3)	− 77.2	1007.4 (− 3.8)	+ 8.3
TBT-CHN (Tibet-China) (25°–45°N; 80°–135°E)	− 1.6 (+ 0.4)	+ 2.5[1]	10,788.6 (− 79.8)	+ 119.8[1]	1006.6 (− 4.5)	− 2.8[1]
CA-IND (central Asia – India) (25°–45°N; 60°–80°E)	0.0 (+ 2.1)	− 1.3	10,818.0 (− 50.0)	− 21.8	1005.0 (− 6.2)	− 1.2
MME (Mediterranean – Middle East) (25°–45°N; 0°–60°E)	− 3.0 (− 0.9)	+ 1.9[5]	10,730.3 (− 138.1)	+ 93.4[5]	1010.7 (+ 0.5)	− 0.7

EC indicates equatorially-conditioned value, and superscripted number percentage level of significance

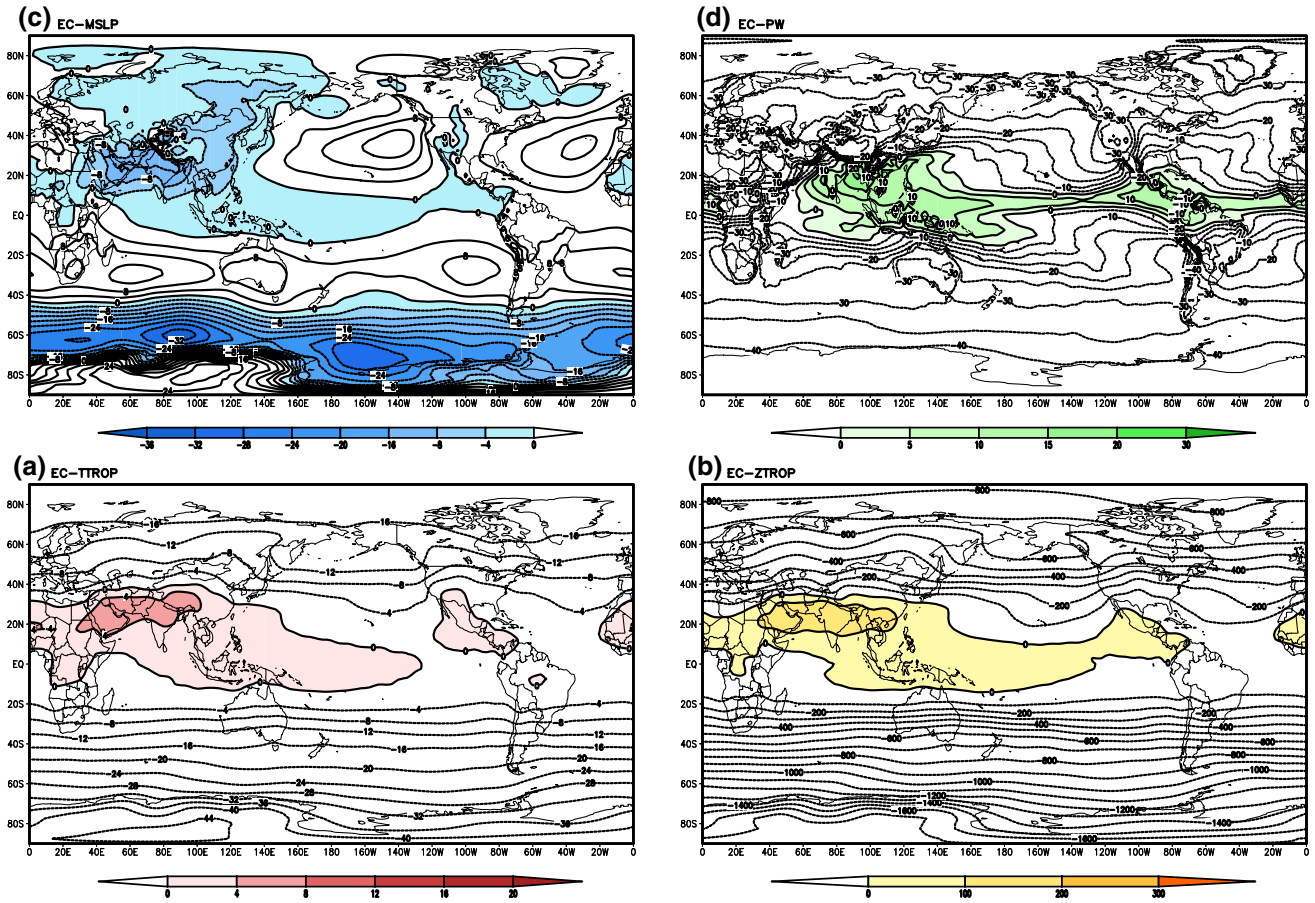

Fig. 2 16–17 June normal global distribution of EC-T_{TROP} (**a**), EC-Z_{TROP} (**b**), EC-mslp (**c**) and EC-PW (**d**)

5.1.3 Pressure

Compared to the equator, pressure (EC-mslp) is higher over the NH (+0.9 mb) and lower over the SH (−0.6 mb), i.e., warmer atmosphere can hold more mass than the cooler one. A huge negative EC-mslp field covers a major portion of the AIP (equatorial Pacific, Indian subcontinent), north tropical Africa and most parts of Eurasia with core (< −12 mb) located over Indo-Gangetic plains (Fig. 2). Different subtropical oceanic highs are distinct and intense (core > +8 to +12 mb). Remaining portion of the entire NH experiences higher pressure condition (EC-mslp positive). The NH higher pressure field is spatially connected with the SH tropical-subtropical positive field over equatorial Atlantic. In other words, the AIP seasonal low-pressure field is surrounded by huge high-pressure field, covering major portion of the globe north of 40 °N latitude through north polar. South subpolar low forms circular zone, south of 40 °S around Antarctica. Three embedded intense cyclonic circulations (core < −24 to −32mb) are indicators of the strength of the convergences across the zone. An isolated higher-pressure field over western Antarctica is intense with core greater than +28mb.

5.1.4 Precipitable water

The EC-PW pattern is heavily loaded over marine areas of the AIP region (around Tibet-Himalaya massif) with two cores (EC-PW > +20 mm), one over Bay of Bengal and another over southeastern China (Fig. 2). The EC-PW decreases to less than −30 mm (< −40 mm) over the NPL (the SPL).

5.2 Global weather regimes (GWRs), streamlines and GC-W_{level}

Normal 16–17 June charts of GWRs, streamlines and GC-W_{level} at four chosen levels (925, 600, 400 and 150 hPa) are given in Fig. 4 for the globe, and in Fig. 5 for extended AIP region. Description of the parameters is, however, based on features at all 12 selected levels. At 1000-hPa, the largest warm-low condition occurs over Afroeurasia-Indo-Pacific region. On east/northeast and south, it is surrounded by

spatially connected cool-high regimes of North Pacific, North Atlantic, north polar and south subtropic. Over Eurasian and adjoining Arctic in the north, the cool-low condition occurs. South temperate-subpolar zone (40°–85°S) experiences cool-low condition and Antarctica cool-high. Size of the warm-low regime decreases upward and is confined over the Indian domain at 400 hPa. Similarly, the cool-high regime shrinks to a narrow zone bounded

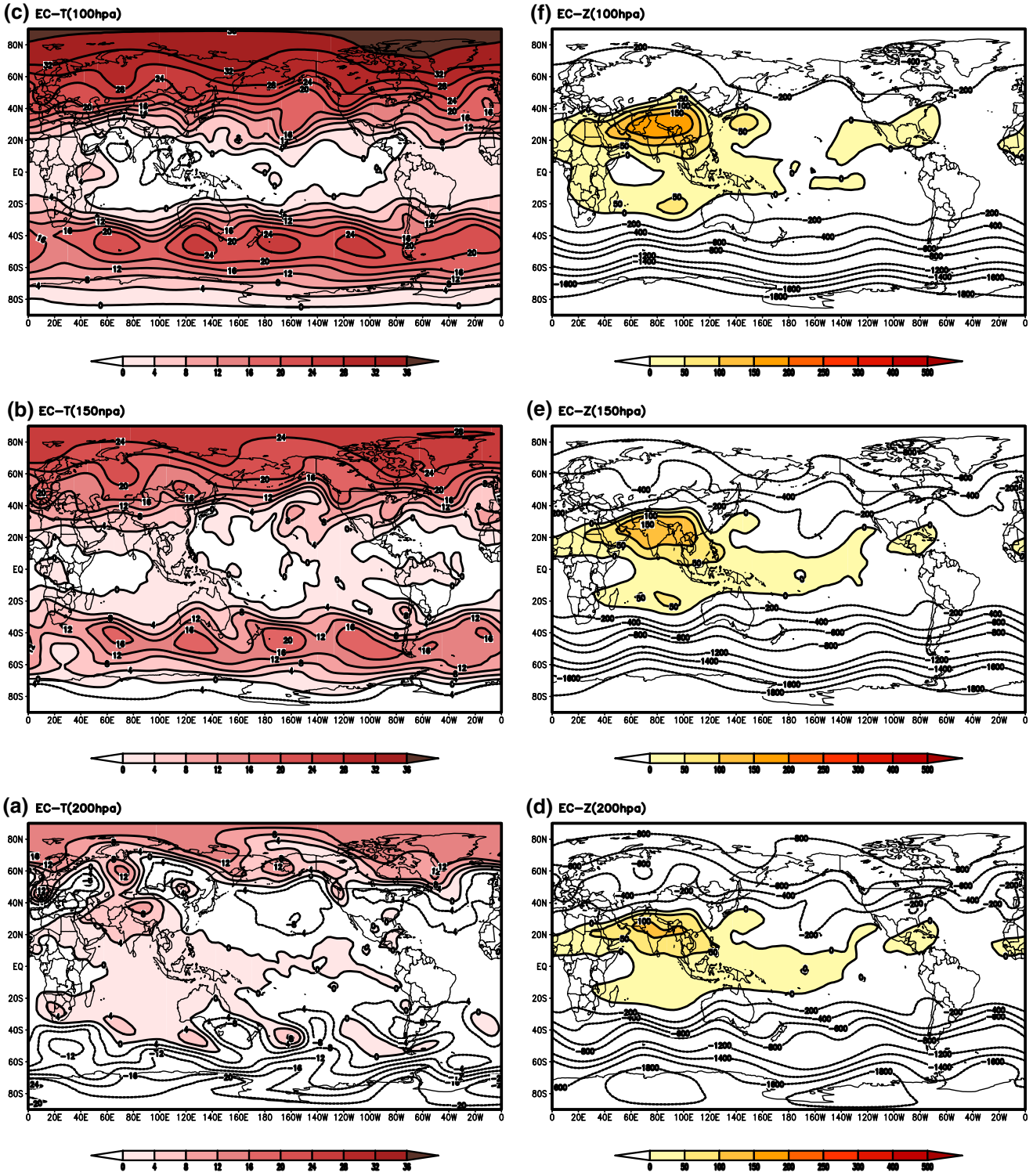

Fig. 3 16–17 June normal global distribution of EC-T_{200} (**a**), EC-T_{150} (**b**), EC-T_{100} (**c**), EC-Z_{200} (**d**), EC-Z_{150} (**e**), and EC-Z_{100} (**f**)

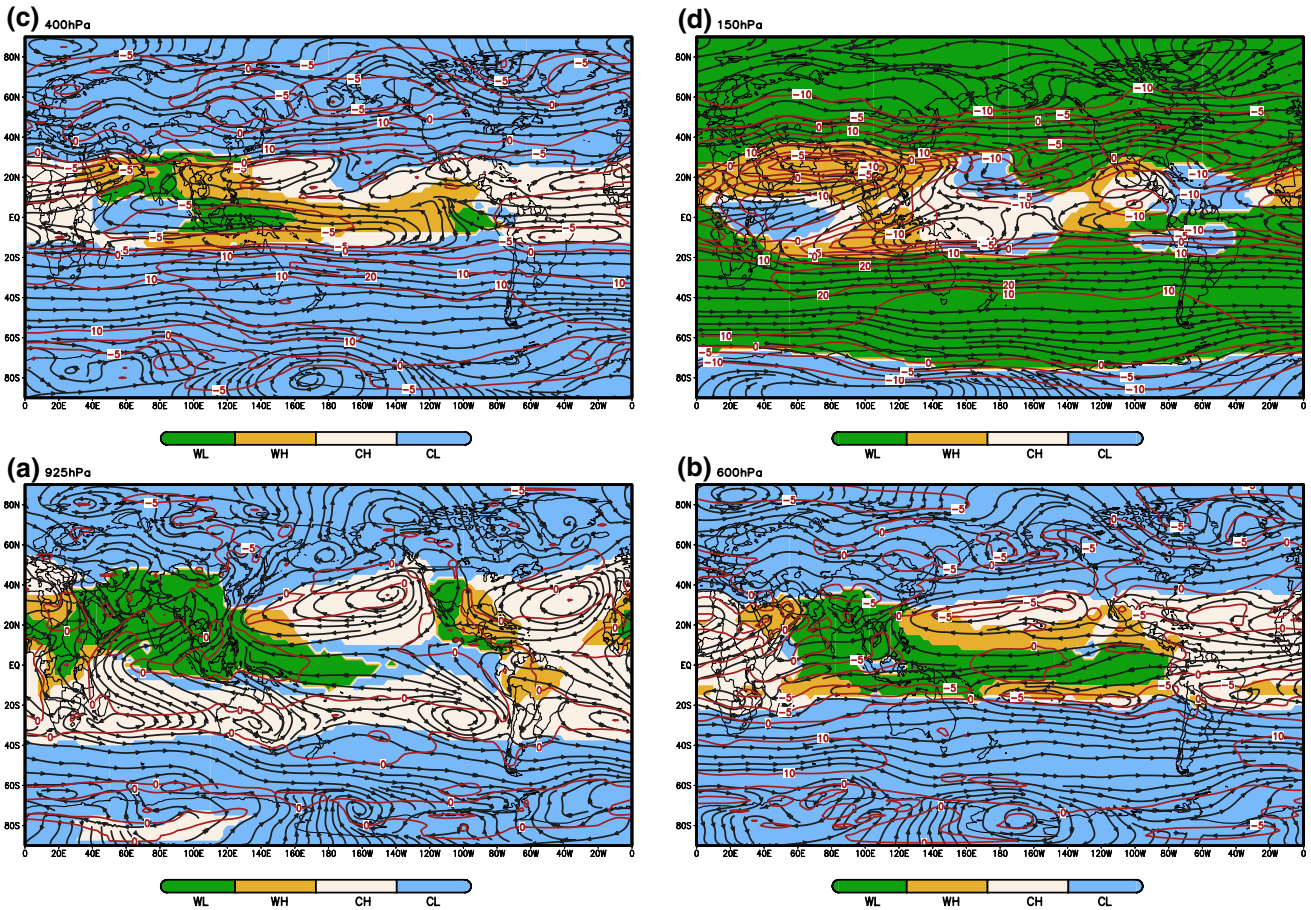

Fig. 4 16–17 June normal global distribution of GWR, streamlines and GC-W_{level} at 925 hPa (**a**), 600 hPa (**b**), 400 hPa (**c**) and 150 hPa (**d**)

by 20 °S–40 °N parallels. On the other hand, the cool-low regimes over the NH and the SH expand upward, and at 400 hPa areas, north of 40 °N and south of 10 °S experience cool-low condition. Above 400 hPa, size of the warm-high regime increases, and at 250 hPa it covers the region from central Pacific through subtropical Afroasia. Upper tropospheric warm-high grows further at upper levels and expand over western North Pacific and North Atlantic. At 100 hPa, however, while intensifying a portion of the warm-high changes to cool-high over western equatorial Pacific-South China Sea-Indochina-southern Saudi Arabia. Remaining portion of the NH and the SH experiences warm-low condition (Figs. 4, 5).

Up to 850 hPa, cross-equatorial Indian Ocean southwesterlies sweep the entire Indian domain (Arabian Sea, Indian contiguous landmass and Bay of Bengal). Major portion of the flows collide with Eurasian westerlies and form east–west oriented convergence zone over Tibetan plateau, while remaining portion confluence with Pacific easterlies and the combined flows exit towards eastern China-Pacific region through arch-passage between Tibet plateau and North Pacific high, where they confluence with straight-flowing Eurasian westerlies and all the flows eventually converge into Aleutian low (Figs. 4, 5). In the 700–500 hPa layer, a portion of Eurasian westerlies form a whirlpool-type cyclonic circulation over Indian domain embedded in the east–west oriented trough over northern Arabian Sea-through South China Sea. Some part of the westerlies drifting from the whirl-pool converge into Tibetan convergence zone, and remaining exit towards China-Pacific region and confluence with straight-flowing Eurasian westerlies. Vertical depth of the convergence zone over Indian domain extends up to 400 hPa. In the 300–200 hPa layer, outflows from the upper tropospheric anticyclonic circulation are mostly directed southwards, a portion of which subside over southern subtropical highs and remaining over south polar. At 150 and 100 hPa levels, the outflows from the anticyclonic circulation blow towards eastern Africa and North Atlantic Ocean. The monsoon Easterly Jetstream is seen at these levels due to squeezing/channelization of the easterlies between Afroasian high and southern subtropical highs (Figs. 4, 5).

Across the NH, horizontal wind field (GC-W_{level} negative) displays meandering/wavy pattern through the full depth of

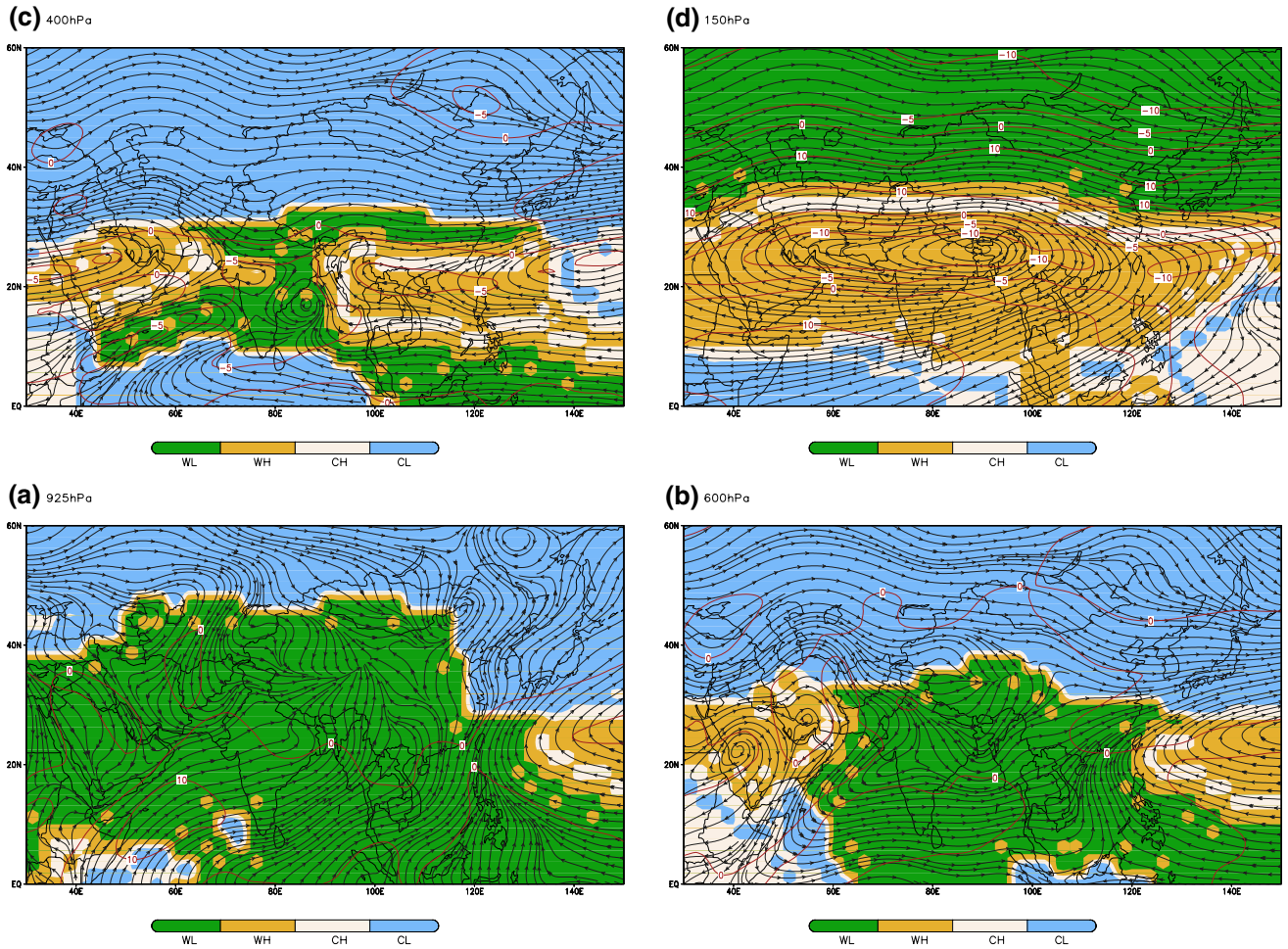

Fig. 5 16–17 June normal regional distribution of GWR, streamline and GC-W_{level} at 925 hPa (**a**), 600 hPa (**b**), 400 hPa (**c**) and 150 hPa (**d**)

1000–100 hPa layer, except over poleward of North Pacific high, where the wind is straight-flowing at 700 hPa (core of GC-W_{700} > + 5 m/s). Over northern North Pacific, the wind speed increases upward and attains peak (core > + 15 m/s) at 250–200 hPa. Further upward (100 hPa), the wind speed decreases and again displays meandering/wavy pattern. Across the SH also, the winds are largely meandering/wavy type. However, intense straight-flowing winds occur over two zones in two different layers. Over southern mid-latitudes (south of Indian Ocean), straight-flowing winds (core > + 4 m/s) occur at 1000 hPa, the speed increases to + 20 m/s at 200 hPa and remains so at upper levels. In southern subtropic, straight-flowing wind emerges at 700 hPa (core > + 5 m/s) over South Pacific. While shifting core location eastward, the speed increases upward and reaches greater than + 30 m/s over Australia at 250–200 hPa but decreases to + 10 m/s to + 20/s at 100 hPa. Interesting to note that outflows from Afroasian anticyclonic circulation in the layer 400–200 hPa are mostly directed southwards which subside south of southern subtropical high and increase the wind speed there. At 150 hPa, the outflows start blowing towards northern Africa, and Jetstream (core > + 15 m/s) is produced over southwest Arabian Sea because of squeezing of the wind flows. The core of the Jetstream shifts over the south of Sri Lanka at 100 hPa (Figs. 4, 5).

5.3 Normal area under Indian monsoon condition during 15–18 June

Identified using the criteria: EC-$T_{1000–700}$ and EC-PW positive and EC-Z_{600} and EC-mslp negative, normal daily area under Indian monsoon condition (AUIMC) during 15–18 June is shown in Fig. 6. The entire South China Sea and Indochina, and major portion of the Indian domain is under Indian monsoon condition by 15–18 June. However, northwestern and extreme northern India (including Uttarakhand State) is not well covered by the AUIMC.

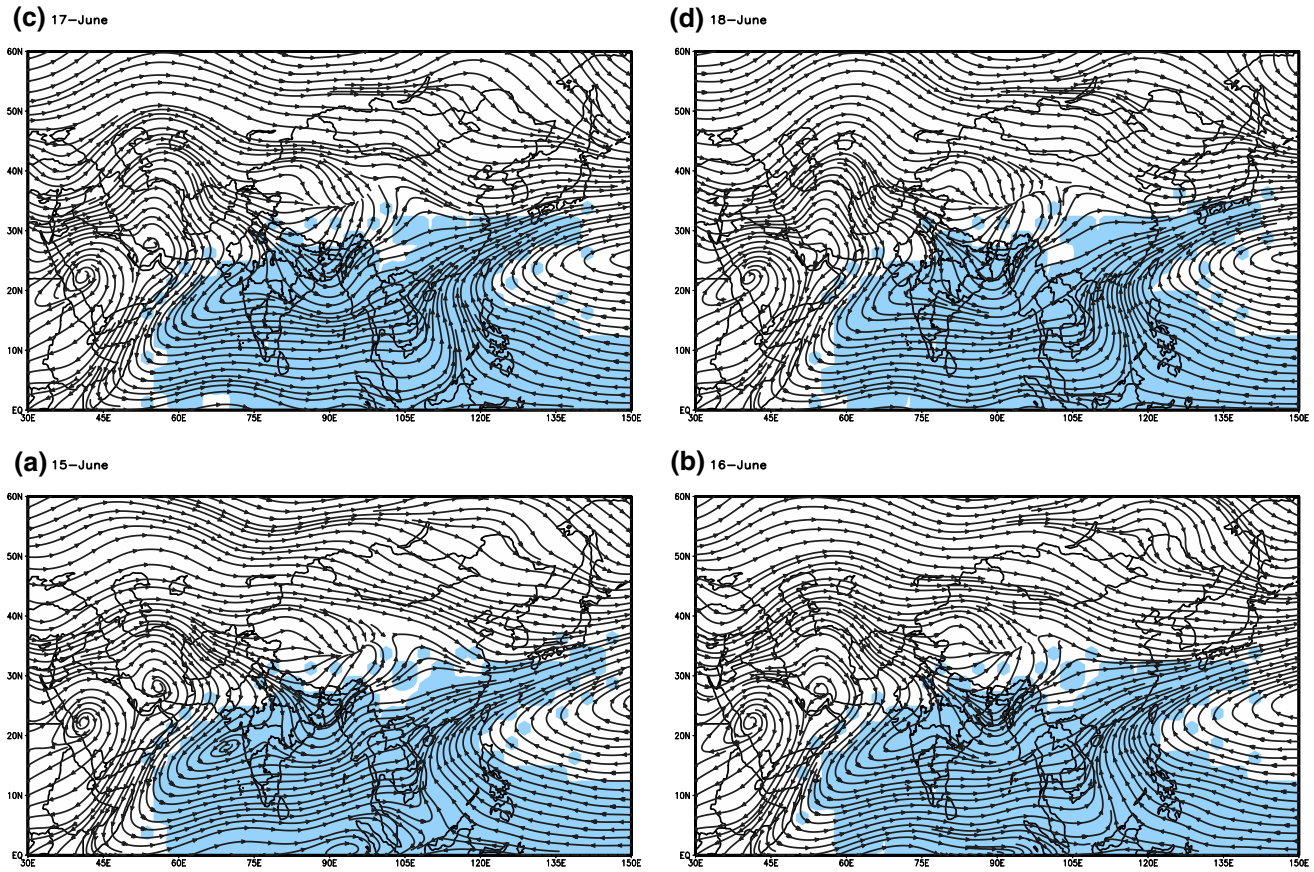

Fig. 6 Normal daily area under Indian monsoon condition and 600-hPa streamlines during 15-18 June

6 Departure-from-normal atmospheric temperature and circulation structures on 16–17 June 2013

6.1 Temperature, height/thickness, pressure and precipitable water

6.1.1 T_{TROP}/Z_{TROP}

The troposphere was warmer-thicker than normal over the NH (+0.6 °C/+26.8 m) and near-normal over the SH (Table 2). It was near-normal over the NPL also, but cooler-thinner over the SPL (−1.6 °C/−77.2 m). However, the troposphere was highly significantly (1% level) warmer-thicker over the TBT-CHN (+2.5 °C/+119.8 m) followed by significantly (5% level) warmer-thicker over the MME (+1.9 °C/+93.4 m) but considerably cooler-thinner over the CA-IND (−1.3 °C/−21.8 m). Furthermore, downward slopes in the tropospheric temperature and thickness from the TBT-CHN to the whole globe, the two hemispheres and nine climatic zones was significantly (at 5–1% level) steeper than normal (Table 3).

Global charts of the departures showed that the troposphere was warmer-thicker over major portions of the globe from south temperate through north subpolar, and cooler-thinner over a relatively smaller portion (Fig. 7a, b). Closer examination revealed that anomalous positive T_{TROP}/Z_{TROP} departures occurred over large continuous geo-domain from TBT-CHN through Russia and northwestern North America. Relatively weaker positive departures occurred over MME and northern Africa. The two areas with warmer-thicker troposphere were separated by central Asia-India sector with cooler-thinner troposphere, which was spatially well connected with negative departure areas of north subpolar-polar, Greenland, northeastern North Atlantic and northwestern Europe. The troposphere was warmer-thicker, though weaker, uniformly across entire tropical-subtropical zones. Over the SH, cooler-thinner troposphere occurred over temperate-subpolar regions, and warmer-thicker across polar region.

At upper levels, broadly size of the area with positive (negative) temperature (height) departure decreased (increased) upward, while that of negative (positive) temperature (height) departure increased (decreased). To get insight into 3D structure of T and Z anomalies, levelwise

Table 3 Normal tropospheric temperature and thickness downward slopes from Tibet-China (TBT-CHN) to indicated geographical units during 16–17 June, and departure-from-normal (DFN) therein during 16–17 June 2013

Geographical units	Tropospheric temperature T_{TROP} (°C)		Tropospheric thickness Z_{TROP} (m)	
	Normal	DFN	Normal	DFN
GLB (globe)	8.4	$+2.3^{1}$	291.0	$+106.2^{1}$
NH (north hemisphere)	4.8	$+2.0^{1}$	148.5	$+93.0^{1}$
SH (south hemisphere)	12.1	$+2.6^{1}$	433.4	$+119.5^{1}$
NPL (north polar; 70°–90°N)	18.5	$+2.5^{5}$	698.5	$+121.4^{1}$
NMLat (north mid-latitudes; 45°–70°N)	12.3	$+2.0^{5}$	460.4	$+97.9^{5}$
NSBT (north subtropic; 25°–45°N)	3.1	$+1.8^{1}$	92.1	$+81.4^{1}$
NTP (north tropic; 2.5°–25°N)	−0.2	$+2.0^{1}$	−64.7	$+95.3^{1}$
EQU (equator; 2.5°S–2.5°N)	0.4	$+1.8^{5}$	−79.8	$+110.4^{5}$
STP (south tropic; 2.5°–25°S)	2.0	$+2.0^{1}$	13.1	$+92.2^{1}$
SSBT (south subtropic; 25°–45°S)	12.2	$+2.4^{1}$	453.5	$+110.9^{5}$
SMLat (south mid-latitudes; 45°–70°S)	23.9	$+3.6^{1}$	928.5	$+161.2^{1}$
SPL (south polar; 70°–90°S)	37.5	$+4.2^{5}$	1421.6	$+197.0^{1}$

Superscripted number indicates percentage level of significance

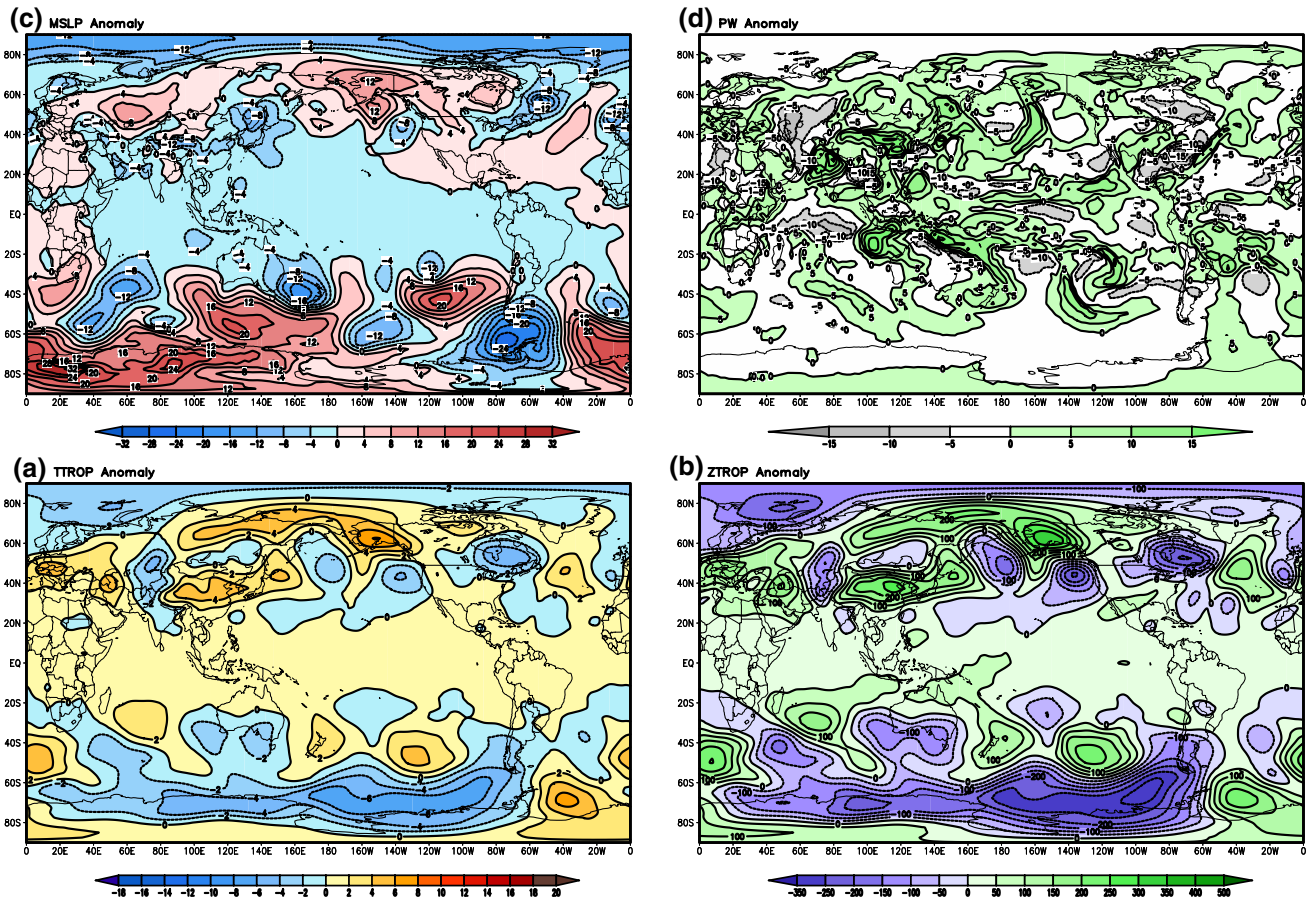

Fig. 7 Global distribution of departure from normal in T_{TROP} (**a**) and Z_{TROP} (**b**), mslp (**c**) and PW (**d**) during 16-17 June 2013

global distribution of departures have been examined. A consolidation of chief features of the pattern was as follows:

1. At 1000 hPa, areas under warmer and cooler conditions were nearly half-way through. Size of the warmer area

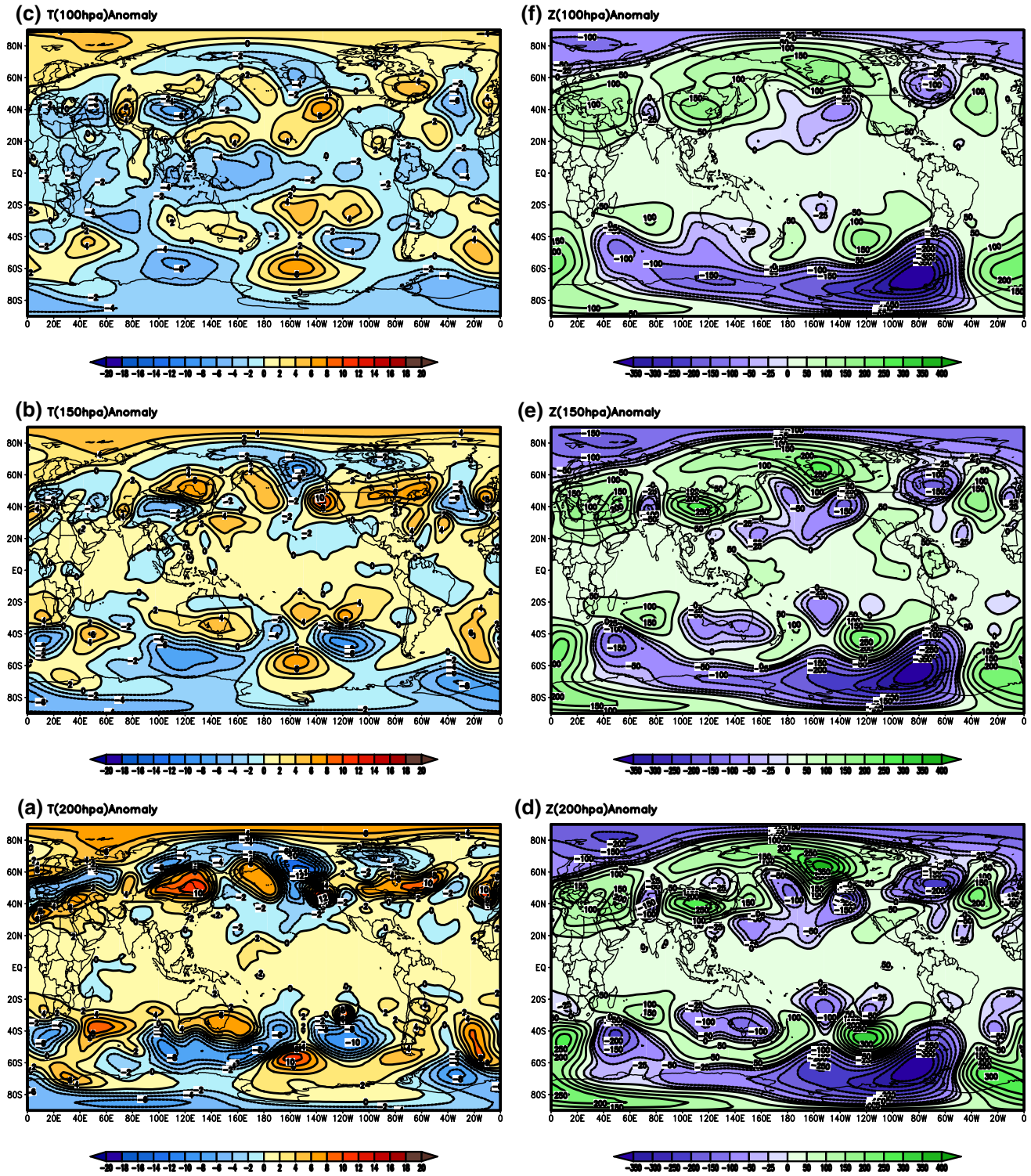

Fig. 8 Departure in T_{200} (**a**), T_{150} (**b**), T_{100} (**c**), Z_{200} (**d**), Z_{150} (**e**) and Z_{100} (**f**) during 16-17 June 2013

increased upward and was largest at 150 hPa (Fig. 8a, b). At 100 hPa, cooler area was the largest (Fig. 8c).

2. Area of negative height departure was largest at 1000 hPa covering parts of Indo-Pacific, entire north polar and adjacent subpolar and considerable portion of south temperate, and positive over remaining parts (north tropical-subtropical and south temperate-polar). This scenario started reversing upward, and at 100 hPa, positive departure occupied most parts of the globe, and negative departure only limited area (north polar-subpolar and south temperate-polar) (Fig. 8d–f).
3. At 1000 hPa, positive temperature and negative height departures occurred over the AIP region, surrounded by areas with positive temperature and height departures (north subtropic-temperate, south subtropic-temperate, and eastern Pacific, America and Atlantic on the east and western Asia, Europe and Africa on the west). Size of the area with higher temperature and lower height decreased upward up to 300 hPa over Asia-Indo-Pacific region, and that of higher temperature as well as height increased upward over surrounding regions. The troposphere was warmer and thinner over north polar and most parts of south subpolar-polar regions.

Notable features closely relevant to the present investigation were positive temperature departure and negative height departure at different tropospheric levels over extended Indo-Pacific region, and positive temperature as well as height departures in the surroundings.

6.1.2 Pressure

In and around the monsoon regime, pressure departure was negative over a vast geographical domain covering major portion of Australasia-Indo-Pacific region bounded by the parallels 40 °S–60 °N (Fig. 7c). The negative field was surrounded by a continuous stretch of positive fields across northern Africa, central Asia, eastern Russia, northern North Pacific (core > + 12 mb), North America, North Atlantic and southern Africa, and a somewhat isolated but large portion of south temperate-subpolar-polar (multiple cores > + 20 to + 32 mb). North subpolar-polar region experienced negative departure (core < − 12 mb). There was an excellent match between global pressure departure field and corresponding tropospheric temperature and thickness departure fields (Fig. 7).

6.1.3 Precipitable water

The major portion of the global domain, south mid-latitude through north polar was covered with a dense mosaic of positive and negative PW departures, and the core of highest positive PW departure (> + 15 mm) was located over central Indo-Gangetic plains (Fig. 7d). Evidently ample atmospheric moisture was available in the monsoon regime. Excessive moisture was also available outside the monsoon regime, which indicated the change in atmospheric circulations and moisture was transported to other regions during the Kedarnath event.

6.2 Actual GWRs and streamlines and departure in W_{level} on 16–17 June 2013

Global charts of 16–17 June 2013 (00:06UTC 16 June – 00:06 17 June 2013) GWRs, streamlines and departure in W_{level} at four chosen levels (925, 600, 400 and 150 hPa) are shown in Fig. 9, and AIP charts in Fig. 10. Keeping in view features of all the 12 selected levels, their descriptions in three broad layers (1000–850 hPa, 700–400 hPa and 300–100 hPa) are given in order.

6.2.1 1000–850 hPa

The India-Indo-Pacific warm-low regime was excessively stretched towards east/northeast but had lesser than normal spreading over western Tibet – Middle East sector. Different cool-high subtropical high-pressure cells were, though broken, but intense. The warm-high pressure cell over Africa was large and intense. An isolated cool-high pressure field also developed over Kazakhstan. Southern easterlies crossing the equator over Indian Ocean—Indonesia swept the entire Arabian Sea – Philippine sector and collided/converged with Eurasian westerlies across Tibet – China region. Intense Eurasian westerlies after interacting with cross-equatorial flows over the northern Arabian Sea formed a cyclonic circulation over northwestern India. The mixed wind system over western North Pacific was forced to blow westward before partially exiting towards the northeast. North mid-high latitudes westerlies were intense and undulating. An intense cyclonic circulation developed over Kamchatka area from the interaction between southwesterly flows from Indian domain and straight-flowing Eurasian westerlies. At 850 hPa, the wind speed departure exceeded + 5 m/s over the Arctic because of squeezing effect over a ridge. South mid-high latitude westerlies were also intense and undulating, and a series of cyclonic cells developed across the zone with wind departures exceeding + 5 to + 10 m/s. A high-pressure anticyclonic circulation occurred over western Antarctica.

6.2.2 700–400 hPa

Huge westerly trough occurred over Middle East – Arabian Sea – India. Extratropical cool-low regime had deeper than normal equatorward penetration over Middle East – extreme northern India—Tibet, and the India-Indo-Pacific warm-low was excessively stretched east/northeastward. Amplitude

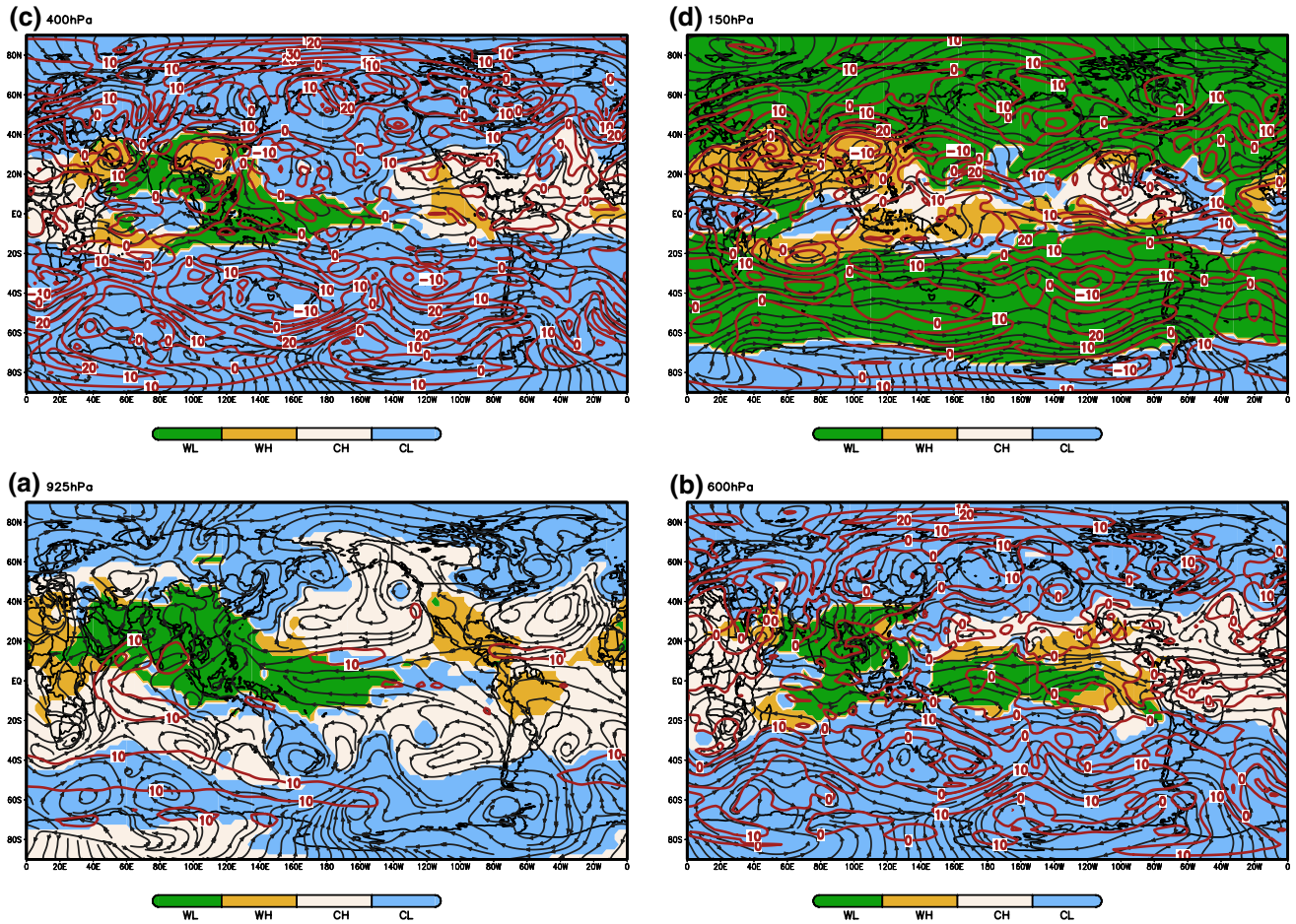

Fig. 9 Global distribution of GWR, streamlines and departure in W_{level} during 06:00 UTC 16 June – 06:00 UTC 17 June 2013 at 925, 600, 400 and 150 hPa

of the westerly trough was lesser at upper levels. Eurasian westerlies after interacting with Indian Ocean southwesterlies and Pacific easterlies (monsoon flows) were forced to blow northwestward parallel to southern slopes of Tibet-Himalaya and to exit towards northern mid-high latitudes from central-western Tibet. The cool-dry westerlies after mixing with warm-moist Indian Ocean southwesterlies and Pacific easterlies pooled huge atmospheric moisture over northwestern India (PW departure exceeded + 15 mm). There was a convergence of three large flows of distinctly different characteristics over western slopes of Tibet-Himalaya massif: (1) cool-dry airs on eastern side of the westerly trough; (2) warm-moist rising airs from convergences across India-Indo-Pacific area; and (3) rotating warm-dry airs of the anticyclonic cell over Tibet-China. Combined effects of cool-dry and warm-moist regime contrast, squeezing of deep warm-moist monsoon wind, lifting of warm-moist flow due to orography and pumping-suction due lower-level convergence and upper level divergence, produced disaster-causing unprecedented monsoon rains over the western slopes of Tibet – Himalaya. After a short spurt of confluencing, converging and condensing, the westerly trough weakened and moved eastward over Tibetan plateau which weakened/destroyed the warm-high TBT-CHN upper tropospheric anticyclonic cell and virtually rainfall activities subsided. Formation and intensification of trough(s) in the westerlies was a short period phenomenon. Therefore, condensation and intense rainfall in subtropical mountainous terrain involving interaction (confluence and convergence) of huge air masses of contrasting characteristics (cool-dry temperate westerlies and warm-moist monsoon winds) was short lived.

The airflows that exited from western-central Tibet-Himalaya bifurcated. The portion that blew toward north polar formed a huge ridge over northeastern Russia – Canada – Greenland sector. Due to squeezing effect, the 400 hPa wind speed (W) departure exceeded + 30 m/s in the core region. Further down, the flows eventually entered into Indian domain via Europe and central Asia. Another portion that blew as westerlies from north of Tibet-Himalaya returned to tropic-equator and converged into the monsoon

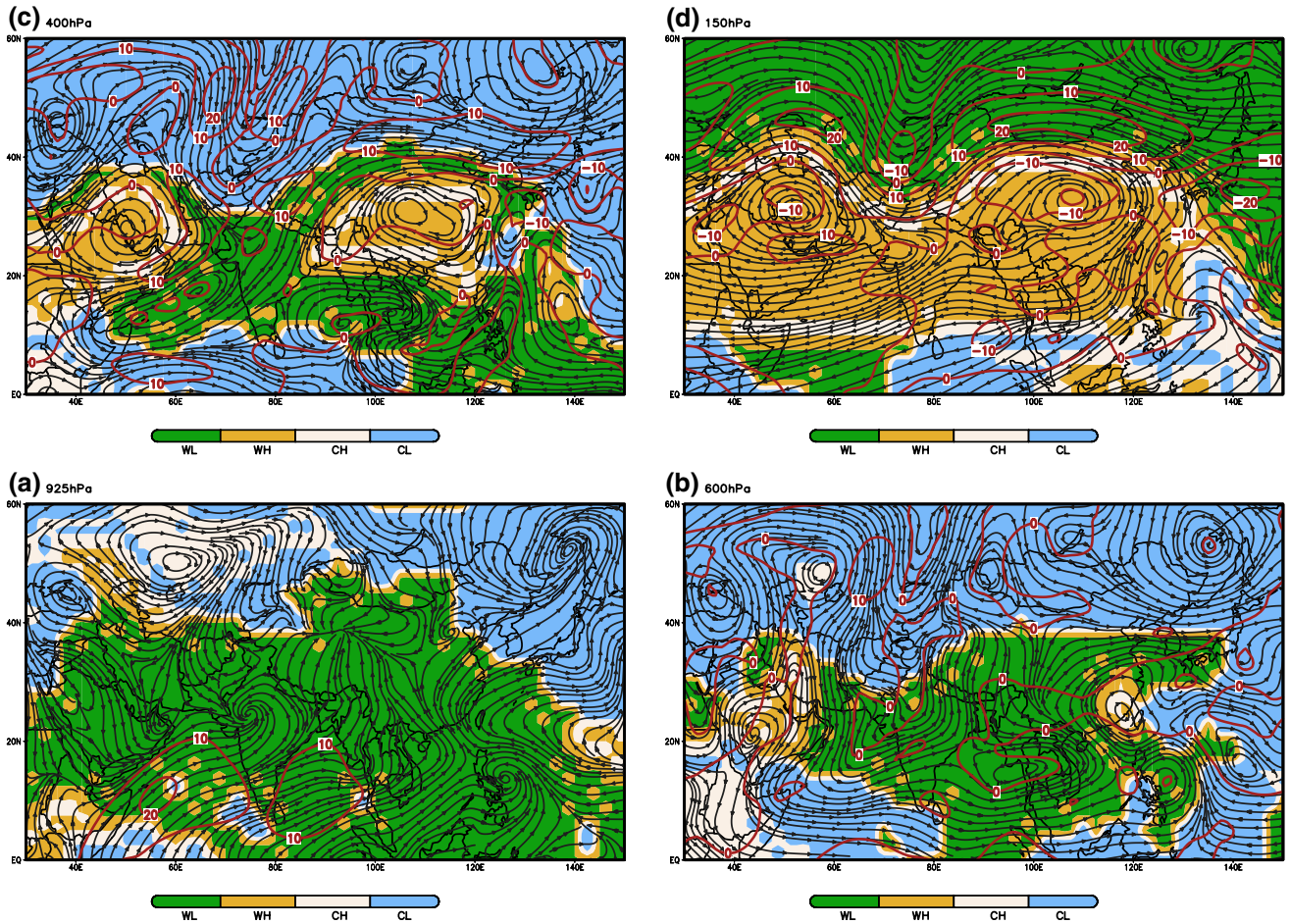

Fig. 10 Regional distribution of GWRs, streamlines and departure in W during 06:00 UTC 16 June – 06:00 UTC 17 June 2013 at 925, 600, 400 and 150-hPa

regime. Due to anticyclonic curvature of the westerlies and subsidence, the North Pacific subtropical high was strengthened and extended/stretched westward up to eastern China, which obstructed the flows exiting towards northeast from Indian domain. From interactions between airs that were drifted equatorward from the right bank of the flows directed toward north polar and that were drifted poleward from the left bank of the straight-flowing westerlies produced series of cyclonic circulations and inclement weathers across the whole of geographical domain between eastern Asia and North America as indicated by isolated pockets of positive PW departure (Fig. 7d). Wind speed departure in the undulating westerlies over the SH was greater than + 20 m/s.

6.2.3 300–100 hPa

In the 300–200 hPa layer, the outflows from the TBT-CHN anticyclonic circulation directed toward north polar returned to the equator via ridge over northeastern Russia – Canada – Greenland sector. At these levels, the north polar was warmer but height was lower due to its integrated value from lower levels. The outflows directed towards east subsided over subtropical North Pacific and North Atlantic, and the return flows from lower levels of the highs converged into monsoon regime. Southward directed outflows subsided partially over the south of southern subtropical high located over South Africa – Australia sector, and remaining over south polar. Wind speed departure in core area of the westerlies over the SH was as: + 5 m/s at 1000 hPa increased to + 20 m/s at 150 hPa and decreased to + 5 m/s at 100 hPa. A thorough examination of levelwise global charts of GWRs, streamlines and wind departures revealed that features of the general and monsoon circulations during Kedarnath disaster were unprecedented.

Due to inherent eastward-shifting tendency of the westerly trough, heavy rain-events in subtropical Asian highlands were short-lived, therefore, popularly known as '*cloud bursts*'. To understand time-evolution of the general and monsoon circulations during the disaster, we have examined different global surface and upper air charts from 1 June

2013 onwards. Changes were mild in the beginning, became organized and intense from 10 June 2013. Abrupt changes started taking place from 14 June 2013, and reached peak (as described above) on 16–17 June 2013.

6.3 The AUIMC at 6-hourly interval during 15–17 June 2013

For extended AIP region, the area under Indian monsoon condition (AUIMC) (criteria: EC-$T_{1000\text{-}700}$ and EC-PW positive, and EC-Z_{600} and EC-mslp negative) and 600 hPa streamline departure at 6-hourly interval during 15 June 2013 (00:00 UTC)–17 June 2013 (18:00 UTC) are shown in Fig. 11. The monsoon condition advanced over Uttarakhand region about 10 days earlier than normal (Fig. 6). Furthermore, the 6-hourly charts showed that ample precipitable water was available in the atmosphere during the event (see also Fig. 7d). In the 600 hPa streamline departure fields, huge extended monsoon trough with a series of embedded cyclonic circulations from western Pacific (west of Philippine) through Indus basin suggested that monsoon circulation was consistently very intense.

7 Mechanism of heavy rains over Kedarnath and impact on global atmosphere

During warmer-thicker troposphere over eastern Tibet—China on 16–17 July 2013, the outflows from intense upper tropospheric anticyclone cell were mostly directed northward and eastward, and partly southward. A huge ridge

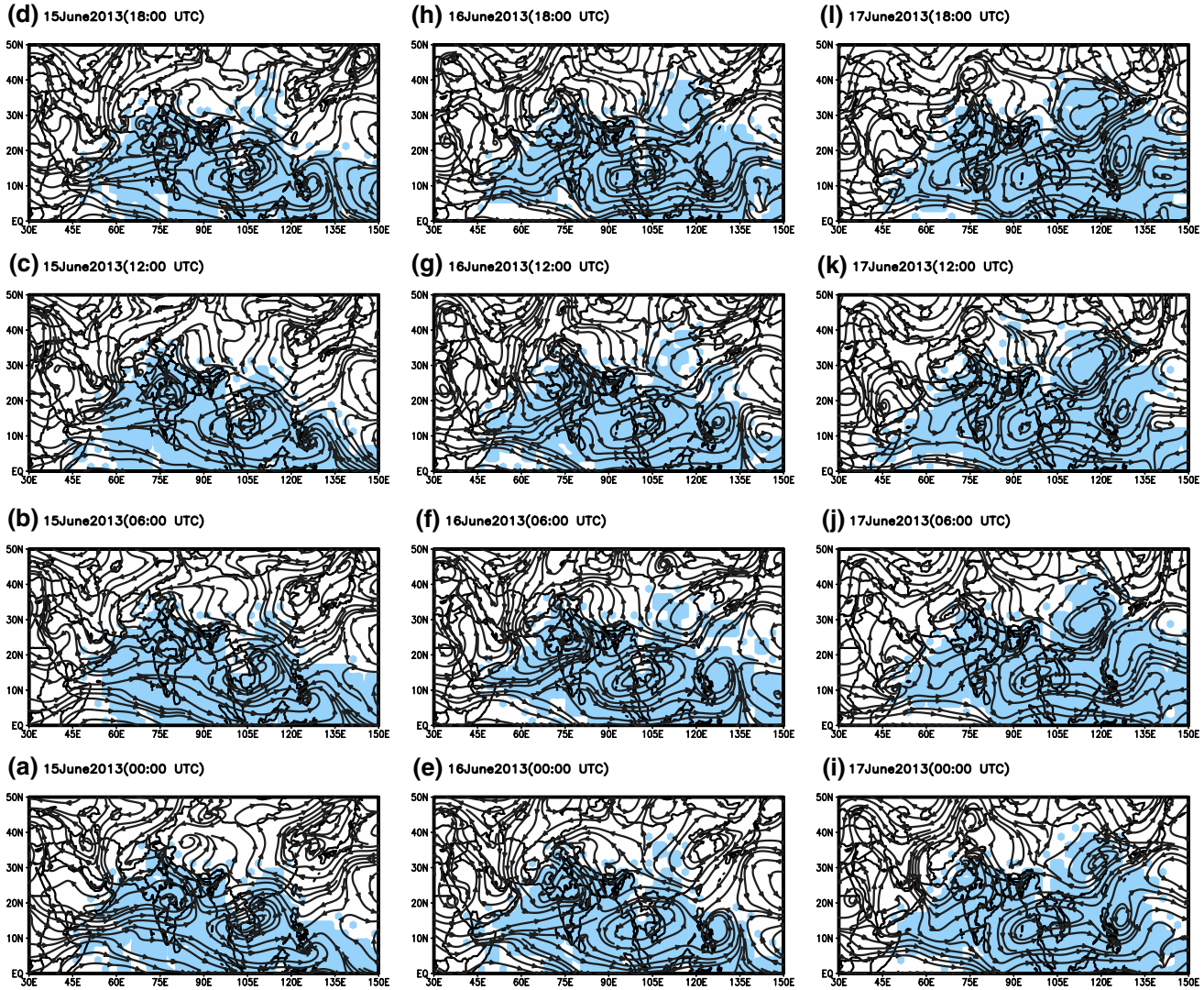

Fig. 11 Area under Indian monsoon condition at 6-hourly interval during 00:00 UTC 15 June – 18:00 UTC 17 June 2013, and 600-hPa departure from normal streamlines

with warmer-thicker troposphere developed over eastern Russia–Canada-Greenland sector, and an anticyclonic circulation over Tibet–China–Pacific sector (Figs. 7, 9). The returnflows from lower levels of the North Pacific high and north polar region joined the equatorial-tropical Pacific easterlies and converged into the monsoon regime. Positive height/thickness departures in lower tropospheric levels over Tibet—China—Pacific partly blocked the exit of the Indian monsoon flows towards eastern China – Pacific sector. Then, the major portion of the monsoon wind started blowing towards the northwest, parallel to southern slopes of the Himalaya, and exited towards mid-high latitudes from western slopes of the Tibet-Himalaya. Three flows with distinctly different characteristics got merged over the western Tibet-Himalaya: (1) cool-dry airs of the westerly trough from northwestern side; (2) warm-moist rising airs from convergences across entire Indo-Pacific domain; and (3) outflowing warm-dry airs of the anticyclonic cell over the TBT-CHN. Combined effects of cool-dry and warm-moist regime contrast, squeezing of deep warm-moist monsoon flows, lifting due to orography and pumping-suction due lower-level convergence and upper level divergence produced disastrous rains over the Kedarnath area. Ample available precipitable water (Figs. 7d, 11) played a crucial role in producing unprecedented rainfall. Voluminous and high-speed wind system from the western Tibet-Himalaya directed towards north mid-high latitudes under the influence of significantly steeper than normal tropospheric temperature and thickness slopes modulated the westerlies pattern into a single wave structure with a huge ridge over eastern Russia – Alaska – Canada sector and a deep trough over Eurasia – Middle East – Indian domain. On eastern side of the ridge, the areas of Greenland – Europe – central Asian in the downstream experienced cooler condition in contiguity with cooler-than-normal north polar region, which deepened the westerly trough over the Middle East—Indian domain. A portion of the airflows from eastern side of the ridge that blew toward equator, strengthened the Atlantic – Pacific equatorial-tropical easterlies, which pushed the deep-moist convection over central-and-western equatorial Pacific westward. This contributed to the intensification of monsoon circulation and rainfall activities. Due to anticyclonic curvature in northwesterlies -westerlies from eastern side of the ridge, which were directed towards Middle East–India, a high-pressure area developed over Europe–western Asia. This high-pressure area got merged with large subtropical high field over the MME region resulting into a huge and deep (extending up to 100 hPa) high-pressure field and an anticyclonic cell over Europe–western Asia–Mediterranean–northern Africa–Middle East. Between the MME high on the west and the TBT-CHN high on the east, the cool/cold westerly trough resembled like a deep gorge. On the other hand, a series of cyclonic circulations evolved across whole of geographical domain between eastern Asia and North America from interactions between airs that drifted equatorward from right bank of the flows directed toward north polar and that drifted poleward from left bank of the straight-flowing westerlies from the TBT-CHN anticyclone. This caused inclement weathers across eastern Asia – northern North Pacific – North Pacific as indicated by anomalous positive PW departures across the domain (Fig. 7d). Earlier reported different causal factors for heavy rains over the Kedarnath area and anomalous circulation features associated with the event, can be traced along the path of unprecedented single-wave structure in the westerly wind fields over the NH, hence interconnected.

The upper tropospheric outflows directed southward mostly subsided over South Africa—Mascarene – South Pacific high sector, and remaining over south polar. The returnflows from south subtropical highs joined and strengthened the equatorial–tropical Pacific easterlies, and contributed to push the warm-moist deep convection from central-western Pacific northwestward over Indian domain. The returnflows from the south polar high blew over Southern, Indian and Pacific Oceans, crossed the equator and eventually converged into the monsoon regime. However, this unusual state of monsoonal and general atmospheric circulations was short-lived as eastward-moving cool/cold westerly trough temporarily weakened/destroyed the TBT-CHN anticyclone, consequently weakened the monsoonal and general circulations. After a short break, warming and thickening of troposphere and intensification of the TBT-CHN upper tropospheric anticyclonic circulation started reviving which heralded a revival of general atmospheric and monsoon circulations. It appeared that during the disaster, the monsoon circulation was divided into two parts – one part that converged around the Tibet-Himalaya and entered into vertical circulation of tropical nature, and another that exited from western Tibet-Himalaya and entered into horizontal meandering flow of extratropical nature.

The departure in pressure and tropospheric temperature and thickness across 54 geo-subdomains across the globe are depicted in Fig. 12. From western Tibet-Himalaya as well as TBT-CHN anticyclone, a large volume of airflows blew over north mid-high latitudes and higher pressure and warmer-thicker troposphere occurred over major portion of the NH. Due to warmer northern hemisphere and change in general circulation, troposphere was warmer-thicker over major parts of south tropic-subtropic. Since, lesser airflows from the TBT-CHN anticyclone were directed towards south polar, anomalous lower pressure and cooler-thinner troposphere occurred over southern mid-high latitudes (south of 45 °S).

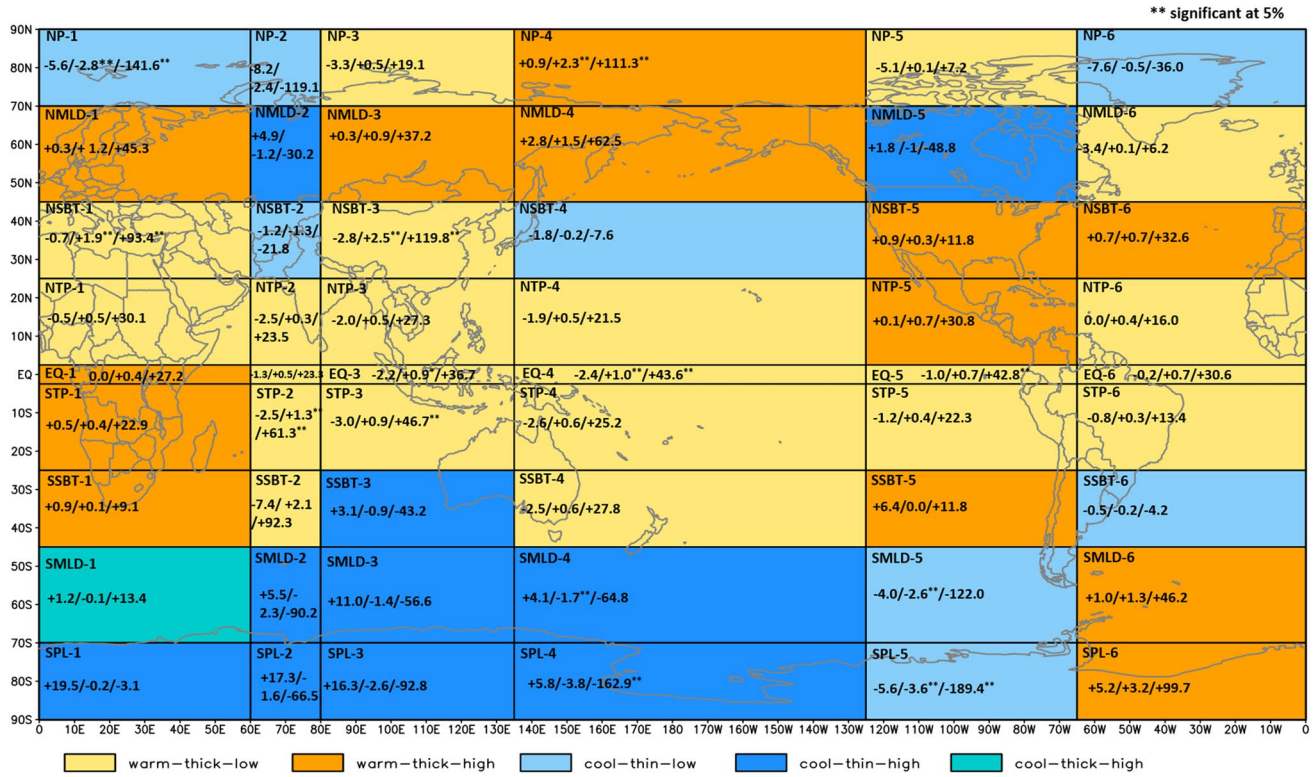

Fig. 12 Departure in mslp, T_{TROP} and Z_{TROP} during 16–17 June 2013 across 54 geographical subdomains. The three parameters are considered in two attributes + ve/−ve: mslp low/high, T_{TROP} warm/cool and Z_{TROP} thick/thin

8 Conclusion

On 16–17 June 2013, the troposphere (1000–250 hPa) was warmer and thicker over the global tropics (25 °S–25 °N). It was warmest and thickest over the Tibet-China (+2.5 °C/+119.8 m), followed by warmer and thicker over the Mediterranean-Middle East (+1.9 °C/+93.4 m, and cooler and thinner in between the two regions, i.e., over central Asia-India (−1.3 °C/−21.8 m). However, the departures in the downward slopes of tropospheric temperature and thickness from Tibet-China to the whole globe, the two hemispheres and different climatic zones were significantly steeper. The monsoon circulation was more intense than normal but the upper tropospheric anticyclonic circulation as a cell was located over Tibet-China sector. In the layer 1000–400 hPa, the India-Indo-Pacific warm-low regime was excessively stretched east/northeastward, while northern mid-high cool-low regime had larger-than-normal equatorward spreading over Middle East – northwestern India – western Tibet. In the upper troposphere (300–100 hPa), two intense, larger size warm-high anticyclonic circulations developed, one over Tibet-China and another over Middle East – Mediterranean. Combined wind system of Eurasian westerlies and Indo-Pacific easterlies over Indian domain was forced to blow westward and make exit from western slopes of Tibet-Himalaya due to higher than normal height of lower tropospheric height fields over Tibet-China sector. Combined effects of five factors over western Himalaya produced disastrous rains over Kedarnath range: (1) intense contrast between north extratropical cool-low-dry regime and monsoon warm-low-moist regime; (2) squeezing of deep warm-moist monsoon flows exiting from western slopes of Himalaya; (3) forced lifting of moist airs due to orography; (4) upward pumping of excessive accumulated moist airs due to intense convergence over northwestern India, and (5) intense suction of airs from lower levels due to intense upper tropospheric divergence over the Tibet-China sector. From western Tibet-Himalaya, voluminous airs in the layer 1000–400 hPa those blew towards north polar modulated mid-high latitudes westerlies into single wave structure with a large ridge over eastern Russia – Canada sector and adjoining Arctic area, and a deep trough over central Asia – India. Besides rainfall, 3D structures of the general and monsoon circulations were also unprecedented since 1979. This is arrived after examining daily EC/GC as well as departure global charts of different parameters from 1 January 1979 through 31 December 2018. Furthermore, different causal factors identified by the researchers for the occurrence of heavy rains over Kedarnath range, as well as other circulation features that were reported to be associated with the

event, were located along the path of a single-waver structure of the westerlies over the NH, hence interconnected. Over major parts of the NH, the troposphere was warmer-and-thicker along upstream of the ridge, while it was cooler-and-thinner in the downstream of the ridge (Fig. 12). From upper trpospheric (300–100 hPa) anticyclonic circulation over Tibet-China, lesser outflows were directed southward and cooler and thinner troposphere occurred over major portions of mid-high latitudes of the SH (south of 45 °S). In other words, the westward blowing lower tropospheric wind over northern India was divided into two parts, one that entered into vertical circulation of tropical nature and another into horizontal meandering flow of extratropical nature.

An adequate number of such investigations would be necessary to draw robust inference on the relationship among 3D global atmospheric thermal structure and general atmospheric and monsoon circulations during extreme rain events across high-and-dry lands of subtropical Asia (Middle East, Himalaya and Tibet).

9 Remarks about application

Real-time analyzed/forecasted charts of equatorially-conditioned (EC) pressure (mslp), precipitable water (PW), and levelwise temperature (T) and height (Z) as well as GWRs, streamlines and globally-conditioned (GC) wind speed (W), are expected to provide adequate visual information to get insight into general and monsoon circulations and rain-producing weather systems. However, one can get still better realistic mental picture of 3D structure of the circulations and weather systems through visualization by preparing charts on the map of proper projection system using sophisticated Geographical Information System (GIS) packages, similar to weather charts given in the website https://www.nullschool.net. Development of GIS-based customized weather charts is a new area of research activity referred to as 'Meteorological Information Systems (MIS) for end-User Meteorologists in Water Sector'. GIS-based charts of numerous other actual and computed parameters, as well as satellite/radar imageries, can also be prepared for advanced scientific researches. The MIS is a step ahead meteorological activity after acquiring model outputs of analyzed and forecasted weather from operational agencies, the customised weather charts are developed according to the requirement of the end-users (agriculture, hydrology, disaster management, aviation, navigation, air pollution etc.).

Acknowledgements First author is extremely gratefully to Director, National Institute of Hydrology, Roorkee for necessary facilities to pursue the study, and to the Department of Science and Technology (DST), Govt. of India for sponsoring this research project.

References

Ashrit R (2010) A report on investigating the Leh cloudburst. NCMRWF report No. NMRF/RR/2010, 18pp

Bohlinger P, Sorteberg A, Sodemann H (2017) Synoptic conditions and moisture sources actuating extreme precipitation in Nepal. J Geophys Res 122(12):653–671

Bohlinger P, Sorteberg A, Liu C, Rasmussen R, Sodemann H, Ogawa F (2019) Multiscale characteristics of an extreme precipitation event over Nepal. Q J R M S 145:179–196. https://doi.org/10.1002/qj.3418

Chaudhari C, Tripathi S, Srivastava R, Misra A (2015) Observation- and numerical -analysis-based dynamics of the Uttarkashi cloudburst. Ann Geophys 33:671–686

Chevuturi A, Dimari AP (2016) Investigation of Uttarakhand (India) disaster-2013 using weather research and forecasting model. Nat Hazards 82(3):1703–1726

Chevuturi A, Dimari AP, Das S, Kumar A, Niyogi D (2015) Numerical simulation of an intense precipitation event over Rudraprayag in the central Himalyas during 13–14 September 2012. J Earth Syst Sci 124(7):1545–1561

Cho C, Li R, Wang S, Yoon JH, Gillies, RR (2015) Anthropogenic footprint of climate change in the June 2013 northern India flood. Plants, Soils, and Climate Faculty Publications. Paper 735, 26pp

Dobhal DP, Gupta AK, Mehta M, Khandelwal DD (2013) Kedarnath disaster: facts and plausible causes. Curr Sci 105(2):171–174

Dube A, Ashrit R, Ashish A, Sharma K, Iyengar GR, Rajagopal EN, Basu S (2014) Forecasting the heavy rainfall during Himalayan flooding-June 2013. Weather Clim Extremes 4:22–34

Dubey CS, Shukla DP, Ningreichon AS, Usham AL (2013) Orographic control of the Kedarnath disaster. Curr Sci 105(11):1474–1476

Hong CC, Hsu HH, Lin NH, Chiu H (2011) Roles of European blocking and tropical-extratropical interaction in the 2010 Pakistan flooding. Geophy Res Lett 38:L13806. https://doi.org/10.1029/2011GL047583

Houze RA, Rasmussen KL, Medina S, Brodzik SR, Romatschke U (2011) Anomalous atmospheric events leading to the summer 2010 floods in Pakistan. Bull Am Meteor Soc 92:291–298

Houze RA, McMurdie LA, Rasmuseen KL, Kumar A, Chaplin MM (2017) Multiscale aspects of the storm producing the June 2013 flooding in Uttarakhand, India. Mon Wea Rev 145(11):4447–4466. https://doi.org/10.1175/MWR-D-17-0004.1

Joseph S, Sahai AK, Sharmila S, Abhilash S, Borah N, Chattopadhyay R, Pillai PA, Rajeevan M, Kumar A (2015) North Indian heavy rainfall event during June 2013: diagnostics and extended range prediction. Clim Dyn 44:2049–2065

Kotal SD, Roy SS, Bhowmik SKR (2014) Catastrophic heavy rainfall episode over Uttarakhand during 16–18 June 2013—observational aspects. Curr Sci 107(2):234–245

Krishnamurti TN, Kumar V, Simon A, Thomas A, Bhardwaj A, Das S, Sen Roy S, Roy Bhowmik RK (2017) March of buoyancy elements during extreme rainfall over India. Clim Dyn 48:1931–1951

Kumar A, Houze RA, Rasmussen KL (2014) Simulation of a flash flooding storm at the steep edge of the Himalyas. J Hydrometeorol 15:212–228

Lau W, Kim KM (2012) The 2010 Pakistan and Russian heat wave: teleconnection of hydro -meteorological extremes. J Hydrometerol 13:392–403

Martha TR, Roy P, Govindraj KB, Kumar V, Diwakar PG, Dhadwal VK (2015) Landslides triggered by the June 2013 extreme rainfall event in parts of Uttarakhand state, India. Landslides 12:135–146

Mishra A, Srinivasan J (2013) Did a cloud burst occur in Kedarnath during 16 and 17 June 2013? Curr Sci 105(10):1351–1352

NATMO (1986) National Atlas of India Physiographic Regions of India. Third edition, Plate 41, Prepared under the Direction of G.K. Dutt, Director, NATMO (the National Atlas & Thematic Mapping Organization), Kolkata, India

Parida BR, Behera SN, Bakimchandra O, Pandey AC, Singh N (2017) Evaluation of satellite-derived rainfall estimates for an extreme rainfall event over Uttarakhand, Western Himalayas. Hydrology 22(4):1–18. https://doi.org/10.3390/hydrology4020022

Priya P, Krishnan R, Mujumdar M, Houze RA Jr (2017) Changing monsoon and midlatitude circulation interactions over the Western Himalayas and possible links to occurrences of extreme precipitation. Clim Dyn 49:2351–2364

Rajeevan M, Bhate J (2008) A high resolution daily gridded rainfall Data Set (1971–2005) for Mesoscale Meteorological Studies. National Climate Center, India meteorological Department, Research Report No.9, 14pp

Ranade A, Singh N (2019) Equatorially/Globally conditioned meteorological analysis of heaviest rains over India during 23–28 July 2005. Meteorol Atmos Phys 131(4):919–944. https://doi.org/10.1007/s00703-018-0613-6

Ranalkar MR, Chaudlhari HS, Hazra A, Sawaisarje GK, Pokhrel S (2016) Dynamical features of incessant heavy rainfall event of June 2013 over Uttarakhand, India. Nat Hazards 80:1579–1601

Rasmussen KL, Houze RA (2012) A flash-flooding storm at the steep edge of high terrain: disaster in the Himalayas. Bull Am Met Soc 93:1713–1724

Rasmussen KL, Hill AJ, Toma VE, Zuluaga MD, Webster PJ, Houze RA (2015) Multiscale analysis of three consecutive years of anomalous flooding in Pakistan. Quart J R Met Soc 141:1259–1276

Ray C, Chattoraj PK, Bisht SL, MPS et al (2016) Kedarnath disaster 2013: causes and consequences using remote sensing inputs. Nat Hazards 81:227–243

Saha S et al (2010) The NCEP climate forecast system reanalysis. Bull Am Meteorol Soc 91(8):1015–1057. https://doi.org/10.1175/2010BAMS3001.1

Saha S et al (2014) The NCEP climate forecast system version 2. J Clim 27:2185–2208. https://doi.org/10.1175/JCLI-D-12-00823.1

Sati VP (2013) Extreme weather-related disasters: a case study of two flash floods hit areas of Badrinath and Kedarnath valleys, Uttarakhand Himalaya, India. J Earth Sci Engg 3:562–568

Shekhar MS, Pattanayak S, Mohanty UC, Paul S, Sravana Kumar SM (2015) A study on the heavy rainfall event around Kedarnath area (Uttarakhand) on 16 June 2013. J Earth Syst Sci 124(7):1531–1544

Singh D, Horton DE, Tsiang T, Haugen M, Ashfaq M, Mei R, Rastogi D, Johnson NC, Charland A, Rajaratnam B, Diffenbaugh NS (2014) Severe precipitation in Northern India in June 2013: causes, historical context, and changes in probability. Bull Am Meteorol Soc 95(9):558–561

Srinivasan J (2013) Predicting and managing extreme rainfall. Curr Sci 105:7–8

Thayyen R, Dimri AP, Kumar P, Agnihotri G (2013) Study of cloudburst and flash floods around Leh, India during August 4–6, 2010. Natur Hazards 65(3):2175–2204

Vellore RK, Kaplan ML, Krishnan R, Lewis JM, Sabade S, Deshpande N, Singh BB, Madhura RK, Rama Rao MVS (2016) Monsoon-extratropical circulation interactions in Himalayan extreme rainfall. Clim Dyn 46:3517–3546

Vellore RK, Bisht JS, Krishnan R, Uppara U, Capua GD, Coumou D (2019) Sub-synoptic circulation variability in the Himalayan extreme precipitation event during June 2013. Meteorol Atmos Phys. https://doi.org/10.1007/s00703-019-00713-5

Webster PJ, Toma VE, Kim HM (2011) Were the 2010 Pakistan floods predictable? Geophys Res Lett 38:L04806